Analytical Regularization Approach to Plane Wave Diffraction From Circular Hole in Infinite Resistive Plane

Mario Lucido, *Senior Member, IEEE*, and Alexander I. Nosich, *Fellow, IEEE*

***Abstract*— In this article, the diffraction of a plane wave from a circular hole in an infinite resistive plane is addressed. In contrast to the holed perfectly electrically conducting (PEC) screens, neither the equivalence principle combined with the image theory nor the Babinet principle can be applied here, and the problem has to be solved directly. The method adopted in this article belongs to the family of methods of analytical preconditioning. The revolution symmetry allows us to reduce the problem to an infinite set of dual integral equations in the vector Hankel transform (VHT) domain for suitable unknowns vanishing outside the hole. Such equations are transformed into matrix equations by means of the Helmholtz-Galerkin discretization technique. The orthogonal eigenfunctions of the most singular part of the integral operator, reconstructing the behavior of the fields at the edge and around the center of the hole, are selected as expansion functions, thus leading to fast converging Fredholm second-kind matrix equations, whose elements can be expressed as quickly evaluable proper integrals. Numerical results show the near-field and far-field characteristics for various cases; the in-house software code is validated by means of comparisons with general-purpose commercial software.**

***Index Terms*— Circular hole, Helmholtz-Galerkin technique, method of analytical preconditioning, plane-wave diffraction, resistive plane.**

I. Introduction

THE diffraction from a hole in an infinite perfectly electrically conducting (PEC) screen represents one of the most popular among the classical problems in electromagnetic theory. Starting from the famous paper by future Lord Rayleigh [1], which dates from the late 19th century, much effort has been devoted to this subject up to the present day. The techniques proposed in the huge number of papers published range from the asymptotic techniques adopted for electrically large apertures, the Bethe-Bouwkamp model for small apertures, the closed-form solution in terms of oblate spheroidal vector wavefunctions for circular apertures, various semi-analytical and numerical techniques, and the reader can refer to the very-well written books, comprehensive reviews, and recent papers for an overview [2], [3], [4], [5], [6], [7], [8], [9], [10]. What is important to note is that a large part of the produced literature is founded on two approaches. In the first one, the equivalence principle, combined with the image theory, leads to an equivalent problem in which fictitious magnetic surface currents replacing the aperture radiate in the free space. The second approach is based on the electromagnetic form of the Babinet principle, according to which the field diffracted by the hole is related to the field scattered in a suitable complementary problem. It is worth emphasizing that both approaches, resulting in boundary value problems whose unknowns are defined on finite supports, are founded on the PEC nature of the screen and cannot be applied when nonperfect materials are involved.

The analysis of the diffraction from holes in infinite penetrable screens was attempted for the first time by Neugebauer [11], where generalized Bethe conditions were proposed and, in turn, used to calculate approximate solutions of Kirchhoff type. More or less ten years later, Ashour [12] analyzed the problem at hand in the geomagnetic context, i.e., in the static case, by means of dual integral equations formulation. In 2007, the analysis of the diffraction by small circular apertures in screens of finite conductivity was addressed by Popov et al. [13] by means of a perturbation approach generalizing the Kirchhoff theory. Only very recently, a full-wave technique, based on dual integral equations formulation and the method of moments, for the analysis of the field penetration through a circular aperture in a thin resistive plate, however, restricted to the axially symmetric case, have been proposed by Lovat et al. [14].

It can be immediately understood that, despite what happened for PEC-holed infinite screens, the attention of the scientific community to the analysis of the diffraction by holes in absorbing screens has been quite nuanced and certainly discontinuous over the past 70 years. This, in part, should surprise because, undoubtedly, a holed penetrable screen represents a more reasonable approximation of a real problem. On the other hand, this tells that such a problem is tremendously more complicated than the one involving a PEC holed screen because it must be solved directly. Moreover, general-purpose commercial software cannot handle infinite objects

Manuscript received 13 December 2022; revised 13 March 2023; accepted 2 June 2023. Date of publication 16 June 2023; date of current version 4 August 2023. This work was supported in part by the Italian Ministry of University Program "Dipartimenti di Eccellenza 2018–2022" and in part by the European Federation of Academies of Sciences and Humanities in the Context of the European Fund for Displaced Scientists Program. *(Corresponding author: Mario Lucido.)*

Mario Lucido is with the Department of Electrical and Information Engineering, University of Cassino and Southern Lazio, 03043 Cassino, Italy (e-mail: lucido@unicas.it).

Alexander I. Nosich is with the Laboratory of Micro and Nano Optics, Institute of Radio-Physics and Electronics, National Academy of Sciences of Ukraine (NASU), 61085 Kharkiv, Ukraine (e-mail: anosich@yahoo.com).

Color versions of one or more figures in this article are available at https://doi.org/10.1109/TAP.2023.3285299.

Digital Object Identifier 10.1109/TAP.2023.3285299

and accurate numerical simulations require the discretization of large (with respect to the wavelength) volumes or surfaces resulting in a huge cost in terms of computation resources. What has been said so far allows us to conclude that the problem at hand needs to be better investigated.

In this article, the diffraction from a circular hole in an infinite resistive plane is considered. The semi-analytical technique adopted, belonging to the class of the methods of analytical preconditioning [15], [16], has been already successfully applied by the authors to the analysis of propagation, radiation, and scattering problems [17], [18], [19], [20], [21], [22], [23]. A holed resistive plane appears as a reasonable model of the small-thickness with respect to the wavelength and penetrable (i.e., material) plate [24]. Namely, the thin plate can be approximated with a plane and a certain set of the two-side generalized boundary conditions for the electromagnetic field. If, additionally, the plate material is optically dense or highly conductive, then the generalized boundary conditions take the form of resistive conditions. This enables one to reduce the scattering problem to solving a surface integral/integral-differential equation for the effective electric surface current density, i.e., the jump of the tangential to the holed resistive plane component of the magnetic field.

Based on the azimuthal symmetry of the problem, by invoking the Fourier series expansion and the vector Hankel transform (VHT), such an equation can be recast as an infinite set of dual integral equations in the spectral domain for the VHT of the azimuthal harmonics of the effective electric surface current density. In contrast to what happens for the thin resistive disk, the spatial domain counterparts of the unknowns are now defined on infinite support. To overcome this problem, such classical unknowns are, then, replaced by the azimuthal harmonics of an auxiliary function coinciding with the tangential component of the electric field in the hole, however, vanishing outside the hole. In this way, the original second-kind hypersingular integral equations defined on the holed resistive plane, i.e., on infinite support, are replaced by the second-kind singular integral equations confined to the hole. Helmholtz decomposition of the azimuthal harmonics of the auxiliary function leads to the adoption of new scalar unknowns in the spectral domain. It is worth observing that the proposed integral equation formulation includes the case of a holed PEC plane, obtained by setting the resistivity to zero. In that case, the second-kind singular integral equations reduce to first-kind hypersingular ones.

The discretization of the dual integral equations is provided by expanding such unknowns in terms of orthogonal eigenfunctions of the most singular part of the integral operator, reconstructing the behavior of the electric field at the hole rim and at its center, in a classical Galerkin scheme. In this context, Galerkin projection acts as a perfect preconditioner and the resulting matrix equations are of the Fredholm second-kind in l^2, i.e., the approximate solution obtained by truncating the matrix equation tends to be the exact solution of the problem as the truncation order tends to infinity. Moreover, the convergence is even fast, i.e., highly accurate results can be achieved by filling a coefficient matrix of a small size. To conclude, the analytical procedure introduced by Lucido et al. [22] and [23] allows writing the elements of the coefficient matrix as fast converging proper integrals, thus guaranteeing negligible computation times.

The remainder of this article is organized as follows. Section II is devoted to presenting the formulation of the problem, the Helmholtz-Galerkin technique, and the expressions of the near and far diffracted field. In Section III, numerical results are provided. The near-field and far-field characteristics are shown for different values of the radius of the hole, the resistivity, the incidence angle, and the polarization of the impinging plane wave. Moreover, comparisons with the commercial software CST Microwave Studio (CST-MWS) are provided in order to validate the implemented in-house software code. The conclusions are summarized in Section IV and three Appendixes contain auxiliary derivations.

II. Proposed Solution of the Problem

This section is aimed at showing the fundamental steps of the proposed solution. In Section II-A, the problem is formulated in terms of an infinite set of dual integral equations in the VHT domain. Subsequently, in Section II-B, the adopted Helmholtz-Galerkin discretization technique, leading to the Fredholm second-kind matrix equations, is presented. To conclude, in Section II-C, the near- and far-zone expressions of the field diffracted by the hole are derived.

A. Infinite Set of Dual Integral Equations in the VHT Domain

In Fig. 1(a), the geometry of the problem at hand is sketched: an infinite material plate of relative dielectric permittivity ε_r, conductivity σ, and thickness τ, with a circular hole of radius a in the free space is considered. A cylindrical coordinate system (ρ, ϕ, z), with the z axis orthogonal to the plate and the origin located at the center of the hole on the median surface S, and a spherical coordinate system (r, θ, ϕ), such that $\rho = rs_\theta$ and $z = rc_\theta$, where $s_t = \sin t$ and $c_t = \cos t$, are introduced. The scattered field is excited by an impinging plane wave propagating in the upper half-space, $\underline{E}^{\text{inc}}(\underline{r}) = \underline{E}_0 e^{-\text{j}\underline{k}\cdot\underline{r}}$ and $\underline{H}^{\text{inc}}(\underline{r}) = 1/(\omega\mu_0)\underline{k} \times \underline{E}_0 e^{-\text{j}\underline{k}\cdot\underline{r}}$, where $\underline{r}$ identifies the observation point, $\underline{E}_0$ is a constant vector, $\underline{k} = -k_0(s_{\theta_0}c_{\phi_0-\phi}\hat{\rho} + s_{\theta_0}s_{\phi_0-\phi}\hat{\phi} + c_{\theta_0}\hat{z})$, $k_0 = \omega\sqrt{\varepsilon_0\mu_0} = 2\pi/\lambda$ is the free space wavenumber, ω is the angular frequency, ε_0 and μ_0 are the dielectric permittivity and the magnetic permeability of the free space, λ is the free space wavelength, whereas the incidence direction is identified by the angles $\theta = \theta_0$ and $\phi = \phi_0$.

In the half-space above the holed material plate, the total field, $(\underline{E}(\underline{r}), \underline{H}(\underline{r}))$, can be written as the superposition of the incident plane wave, the plane wave reflected by the plate without the hole, $(\underline{E}^{\text{refl}}(\underline{r}), \underline{H}^{\text{refl}}(\underline{r}))$, and the perturbation due to the hole, which is the diffracted field, $(\underline{E}^{\text{diffr}}(\underline{r}), \underline{H}^{\text{diffr}}(\underline{r}))$, i.e., $\underline{E}(\underline{r}) = \underline{E}^{\text{inc}}(\underline{r}) + \underline{E}^{\text{refl}}(\underline{r}) + \underline{E}^{\text{diffr}}(\underline{r})$ and $\underline{H}(\underline{r}) = \underline{H}^{\text{inc}}(\underline{r}) + \underline{H}^{\text{refl}}(\underline{r}) + \underline{H}^{\text{diffr}}(\underline{r})$. Whereas, in the half-space below the holed plate, the total field is given by the superposition of the plane wave transmitted by the plate without

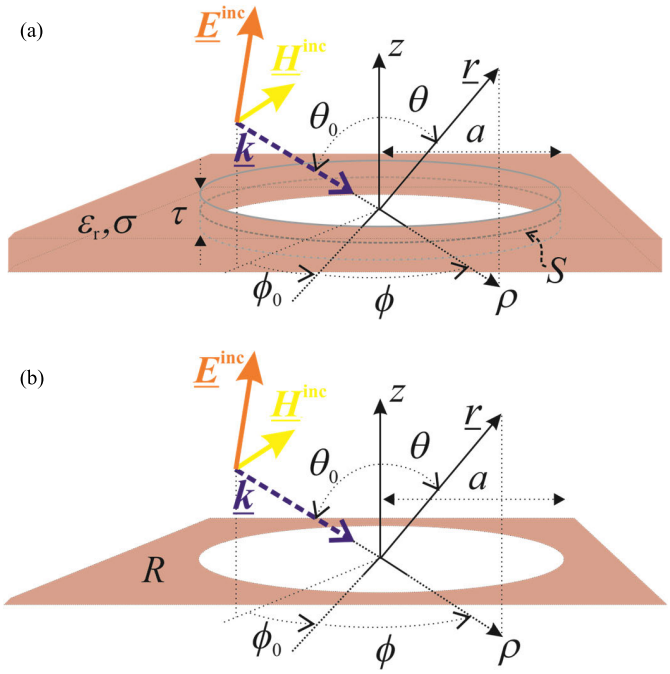

Fig. 1. Geometry of the problem, incident plane wave, and adopted notations. (a) Infinite holed material plate of relative dielectric permittivity ε_r, conductivity σ, and thickness τ. (b) Holed resistive plane of resistivity R.

hole, $(\underline{E}^{\mathrm{tr}}(\underline{r}), \underline{H}^{\mathrm{tr}}(\underline{r}))$, and, again, the perturbation due to the hole, i.e., $\underline{E}(\underline{r}) = \underline{E}^{\mathrm{tr}}(\underline{r}) + \underline{E}^{\mathrm{diffr}}(\underline{r})$ and $\underline{H}(\underline{r}) = \underline{H}^{\mathrm{tr}}(\underline{r}) + \underline{H}^{\mathrm{diffr}}(\underline{r})$. On the other hand, the scattered field, $(\underline{E}^{\mathrm{sc}}(\underline{r}), \underline{H}^{\mathrm{sc}}(\underline{r}))$, is defined as the difference between the total field and the incident field, i.e., $\underline{E}^{\mathrm{sc}}(\underline{r}) = \underline{E}(\underline{r}) - \underline{E}^{\mathrm{inc}}(\underline{r})$ and $\underline{H}^{\mathrm{sc}}(\underline{r}) = \underline{H}(\underline{r}) - \underline{H}^{\mathrm{inc}}(\underline{r})$.

Supposing that $\sigma \gg \omega\varepsilon_0\varepsilon_r$ and $\tau < d_{skin} \ll \lambda$, where $d_{skin} = \sqrt{2/(\omega\mu_0\sigma)}$ is the skin depth, the field inside the plate can be neglected, and the infinite thin material plate can be approximated with a zero-thickness resistive plane located on the median surface S [see Fig. 1(b)]. In that case, the following two-side generalized boundary conditions have to be satisfied by the electromagnetic field on the median surface S [24]:

$$\hat{z} \times \left(\underline{E}\left(\rho, \phi, 0^+\right) - \underline{E}\left(\rho, \phi, 0^-\right)\right) = \underline{0} \tag{1a}$$

$$\frac{1}{2}\hat{z} \times \left(\underline{E}\left(\rho, \phi, 0^+\right) + \underline{E}\left(\rho, \phi, 0^-\right)\right) \times \hat{z} = R\underline{J}\left(\rho, \phi\right) \tag{1b}$$

for $\rho \geq a$ and $0 \leq \phi < 2\pi$, where R is the resistivity (i.e., the surface resistance) of the plane and $\underline{J}(\rho, \phi) = \hat{z} \times (\underline{H}(\rho, \phi, 0^+) - \underline{H}(\rho, \phi, 0^-))$, i.e., the jump across the median surface S of the tangential component of the magnetic field, defines the effective electric surface current density.

Additionally, we assume that the plate material is a good conductor (its conductivity is $\sigma \gg \omega\varepsilon_0\varepsilon_r$), hence, $R = 1/(\sigma\tau)$, i.e., the resistivity is purely real-valued [24]. By imposing the local power boundedness condition and the Silver-Muller radiation condition on the diffracted field, which is possible if R is not a purely imaginary number (see Appendix A), a uniquely solvable boundary value problem for the Maxwell equations is obtained [15], [25]. It is worth noting that, since the plane waves reflected and transmitted by the infinite plane without holes can be simply expressed in closed form, the only unknown quantity in the boundary value problem at hand is the field diffracted by the hole.

By applying the second Green's formula or starting from the integral representation of the vector potential, (1) can be written in terms of a surface integral or, alternatively, integral-differential equation for the effective electric surface current density $\underline{J}(\rho, \phi)$ [26]. As the diffracted field can be represented as a convolution integral involving the free-space dyadic Green's function, the Silver-Muller radiation condition is satisfied automatically if the Green's function satisfies that condition. On the other hand, taking advantage of the revolution symmetry, all the involved functions can be conveniently expanded in the Fourier series. In this way, indeed, due to the orthogonality properties of the azimuthal harmonics, the problem can be equivalently formulated in terms of an infinite set of 1-D integral equations for the azimuthal harmonics of the effective electric surface current density. By invoking the VHT of the order $n \in \mathbb{Z}$ (VHT_n) [27]

$$\tilde{\underline{\mathbf{P}}}^{(n)}(w) = \int_0^{+\infty} \underline{\underline{\mathbf{H}}}^{(n)}(w\rho)\, \underline{\mathbf{P}}^{(n)}(\rho)\, \rho d\rho \tag{2}$$

where

$$\underline{\underline{\mathbf{H}}}^{(n)}(w\rho) = \begin{pmatrix} J_n'(w\rho) & \dfrac{nJ_n(w\rho)}{w\rho} \\ \dfrac{nJ_n(w\rho)}{w\rho} & J_n'(w\rho) \end{pmatrix} \tag{3}$$

is the kernel of the VHT_n, $J_\nu(\cdot)$ and $J_\nu'(\cdot)$ are, respectively, the Bessel function of the first kind and order ν and its first derivative with respect to the argument [28]

$$\underline{\mathbf{P}}^{(n)}(\rho) = \int_0^{+\infty} \underline{\underline{\mathbf{H}}}^{(n)}(w\rho)\, \tilde{\underline{\mathbf{P}}}^{(n)}(w)\, w dw \tag{4}$$

denotes the inverse VHT_n (VHT_n^{-1}) and the symbols

$$\underline{\mathbf{P}}^{(n)}(\rho) = \begin{pmatrix} P_\rho^{(n)}(\rho) \\ -\mathrm{j}P_\phi^{(n)}(\rho) \end{pmatrix} \tag{5a}$$

$$\tilde{\underline{\mathbf{P}}}^{(n)}(w) = \begin{pmatrix} \tilde{P}_{\mathrm{C}}^{(n)}(w) \\ -\mathrm{j}\tilde{P}_{\mathrm{D}}^{(n)}(w) \end{pmatrix} \tag{5b}$$

have been introduced, the nth azimuthal harmonic of the transverse with respect to the z axis and longitudinal, i.e., along the z axis, components of the scattered electric field can be respectively written as follows [29]:

$$\underline{\mathbf{E}}_t^{\mathrm{sc}(n)}(\rho, z) = \int_0^{+\infty} \underline{\underline{\mathbf{H}}}^{(n)}(w\rho)\, \underline{\underline{\tilde{\mathbf{G}}}}(w)\, \tilde{\underline{\mathbf{J}}}^{(n)}(w) \cdot e^{-\mathrm{j}\sqrt{k_0^2 - w^2}|z|} w dw \tag{6a}$$

$$E_z^{\mathrm{sc}(n)}(\rho, z) = -\mathrm{j}\frac{\mathrm{sgn}(z)}{2\omega\varepsilon_0} \int_0^{+\infty} J_n(w\rho)\, \tilde{J}_{\mathrm{C}}^{(n)}(w) \cdot e^{-\mathrm{j}\sqrt{k_0^2 - w^2}|z|} w^2 dw \tag{6b}$$

where $\sqrt{k_0^2 - w^2} = -\mathrm{j}\sqrt{w^2 - k_0^2}$

$$\underline{\underline{\tilde{\mathbf{G}}}}(w) = \begin{pmatrix} \tilde{G}_{\mathrm{C}}(w) & 0 \\ 0 & \tilde{G}_{\mathrm{D}}(w) \end{pmatrix} = \begin{pmatrix} -\dfrac{\sqrt{k_0^2 - w^2}}{2\omega\varepsilon_0} & 0 \\ 0 & -\dfrac{\omega\mu_0}{2\sqrt{k_0^2 - w^2}} \end{pmatrix} \tag{7}$$

is related to the spectral domain, i.e., the w-domain, counterpart of the free-space dyadic Green's function, and $\tilde{\underline{\mathbf{J}}}^{(n)}(w)$ is the VHT$_n$ of the nth azimuthal harmonic of the effective electric surface current density. Hence, the equations in the spatial domain can be replaced by the following infinite set of dual integral equations in the spectral domain:

$$\int_0^{+\infty} \underline{\underline{\mathbf{H}}}^{(n)}(w\rho)\, \tilde{\underline{\mathbf{J}}}^{(n)}(w)\, w dw = \underline{\mathbf{0}}, \quad \text{for } \rho < a \tag{8a}$$

$$\int_0^{+\infty} \underline{\underline{\mathbf{H}}}^{(n)}(w\rho) \left(\underline{\underline{\tilde{\mathbf{G}}}}(w) - R\underline{\underline{\mathbf{I}}}\right) \tilde{\underline{\mathbf{J}}}^{(n)}(w)\, w dw = -\underline{\mathbf{E}}_t^{\mathrm{inc}(n)}(\rho, 0), \quad \text{for } \rho > a \tag{8b}$$

with $n \in \mathbb{Z}$, where the nth azimuthal harmonic of the tangential component of the incident electric field evaluated on the median surface S can be written as follows:

$$\underline{\mathbf{E}}_t^{\mathrm{inc}(n)}(\rho, 0) = -\mathrm{j}^{n+1} e^{-\mathrm{j}n\phi_0} \underline{\underline{\mathbf{H}}}^{(n)}\left(k_0 s_{\theta_0}\rho\right) \underline{\mathbf{E}}_{0t}. \tag{9}$$

Equation (8a) simply states the vanishing of the nth azimuthal harmonic of the effective surface current density in the hole. On the other hand, the hypersingular nature of the second-kind integral equation in (8b), defined on an infinite support ($\rho > a$), can be deduced from the asymptotic behavior of $\underline{\underline{\tilde{\mathbf{G}}}}(w)$.

It is clear that the discretization technique developed in [23] for the plane-wave scattering from a thin resistive disk and, hence, for unknowns and integral equations defined on finite support, cannot be directly applied. To overcome this problem, an alternative integral formulation is devised as follows:

By means of the known identity [30]

$$\int_0^{+\infty} J_n(w\rho_1)\, J_n(w\rho_2)\, w dw = \frac{\delta(\rho_1 - \rho_2)}{\rho_1} \tag{10}$$

it is simple to show that

$$\tilde{\underline{\mathbf{E}}}_t^{\mathrm{inc}(n)}(w, 0) = -\mathrm{j}^{n+1} e^{-\mathrm{j}n\phi_0} \frac{\delta\left(w - k_0 s_{\theta_0}\right)}{w} \underline{\mathbf{E}}_{0t}. \tag{11}$$

Hence, by introducing the auxiliary unknown function $\bar{\underline{J}}(\rho, \phi)$ of nth azimuthal harmonic $\bar{\underline{\mathbf{J}}}^{(n)}(\rho)$ such that

$$\tilde{\bar{\underline{\mathbf{J}}}}^{(n)}(w) = \left(\underline{\underline{\tilde{\mathbf{G}}}}(w) - R\underline{\underline{\mathbf{I}}}\right) \tilde{\underline{\mathbf{J}}}^{(n)}(w) + \tilde{\underline{\mathbf{E}}}_t^{\mathrm{inc}(n)}(w, 0) \tag{12}$$

the dual integral equations (8) can be rewritten as follows:

$$\int_0^{+\infty} \underline{\underline{\mathbf{H}}}^{(n)}(w\rho) \left(\underline{\underline{\tilde{\mathbf{G}}}}(w) - R\underline{\underline{\mathbf{I}}}\right)^{-1} \tilde{\bar{\underline{\mathbf{J}}}}^{(n)}(w)\, w dw = -\frac{1}{R}\underline{\mathbf{E}}_t^{\mathrm{tr}(n)}(\rho, 0), \quad \text{for } \rho < a \tag{13a}$$

$$\int_0^{+\infty} \underline{\underline{\mathbf{H}}}^{(n)}(w\rho)\, \tilde{\bar{\underline{\mathbf{J}}}}^{(n)}(w)\, w dw = \underline{\mathbf{0}}, \quad \text{for } \rho > a \tag{13b}$$

where (see Appendix B)

$$\underline{\mathbf{E}}_t^{\mathrm{tr}(n)}(\rho, 0) = R\mathrm{j}^{n+1} e^{-\mathrm{j}n\phi_0} \underline{\underline{\mathbf{H}}}^{(n)}\left(k_0 s_{\theta_0}\rho\right) \cdot \left(\underline{\underline{\tilde{\mathbf{G}}}}\left(k_0 s_{\theta_0}\right) - R\underline{\underline{\mathbf{I}}}\right)^{-1} \underline{\mathbf{E}}_{0t} \tag{14}$$

is the nth azimuthal harmonic of the tangential component of the transmitted electric field evaluated on the median surface S.

The asymptotic behavior of the kernel in (13a), i.e.,

$$\frac{1}{\tilde{G}_T(w) - R} \overset{w \to +\infty}{\sim} \kappa_T w^{2(p_T - 1)} \tag{15}$$

for $T = \mathrm{C}, \mathrm{D}$, where $\kappa_{\mathrm{C}} = -\mathrm{j}2\omega\varepsilon_0$ and $\kappa_{\mathrm{D}} = -1/R$, $p_{\mathrm{C}} = 1/2$ and $p_{\mathrm{D}} = 1$, reveals the singular nature of the corresponding second-kind integral equation. Moreover, from (4), (6a), (8a), (12), and (13b), it is simple to conclude that the auxiliary unknown function coincides with the tangential component of the electric field in the hole, i.e., $\bar{\underline{J}}(\rho, \phi) = \underline{E}_t(\rho, \phi, 0)$ for $\rho < a$, and vanishes for $\rho > a$. Hence, based on the Fourier series expansion properties and the behavior of the electric field at the edge [31], the following physical behavior of the components of $\bar{\underline{\mathbf{J}}}^{(n)}(\rho)$ can be readily established:

$$\bar{J}_t^{(n)}(\rho) = \begin{cases} \rho^{||n|-1|}(a - \rho)^{p_t} \hat{J}_t^{(n)}(\rho), & \text{for } \rho < a \\ 0, & \text{for } \rho > a \end{cases} \tag{16}$$

for $t = \rho, \phi$, where $p_\rho = -1/2$, $p_\phi = 0$ and $\hat{J}_t^{(n)}(\rho)$ are well-behaved functions. Under this assumption about the functional spaces to which the azimuthal harmonics of the auxiliary unknowns belong, the unique solvability of the dual integral equations (13) can be immediately demonstrated by means of Parseval equality [32].

It is interesting to observe that the proposed integral equation formulation is very general including the case of a holed PEC plane, which can be readily obtained by setting the resistivity to zero. In that case, the second-kind singular integral equation in (13a) reduces to a first-kind hypersingular integral equation. Despite that, the discretization technique described in Section II-B can be applied even in such a case providing to consider the vanishing of the ϕ-components of the unknowns at the edge, which simply requires a different definition of the expansion bases.

B. Regularizing Helmholtz-Galerkin Discretization Technique

An expression in closed form of the solution of the dual integral equations (13) is not available, hence, a discretization scheme has to be adopted to resort to an approximate numerical solution of the problem.

Now, in accordance with the VHT, the trivial choice of the components of $\bar{\underline{\mathbf{J}}}^{(n)}(\rho)$ as independent unknowns in the spatial domain leads to two vector unknowns in the spectral domain. On the other hand, Helmholtz decomposition allows writing $\bar{\underline{\mathbf{J}}}^{(n)}(\rho)$ as the superposition of a surface curl-free contribution,

$\underline{\bar{\mathbf{J}}}_{\mathrm{C}}^{(n)}(\rho) = \begin{pmatrix} d/d\rho \\ n/\rho \end{pmatrix} \Phi_{\mathrm{C}}^{(n)}(\rho)$, and a surface divergence-free contribution, $\underline{\bar{\mathbf{J}}}_{\mathrm{D}}^{(n)}(\rho) = -\mathrm{j} \begin{pmatrix} n/\rho \\ d/d\rho \end{pmatrix} \Phi_{\mathrm{D}}^{(n)}(\rho)$, where $\Phi_T^{(n)}(\rho)$ for $T = \mathrm{C}, \mathrm{D}$ are suitable potential functions [33], the VHT_n of which have only one nonvanishing component [34], i.e.,

$$\underline{\tilde{\bar{\mathbf{J}}}}_{\mathrm{C}}^{(n)}(w) = \begin{pmatrix} \tilde{J}_{\mathrm{C}}^{(n)}(w) \\ 0 \end{pmatrix} \tag{17a}$$

$$\underline{\tilde{\bar{\mathbf{J}}}}_{\mathrm{D}}^{(n)}(w) = \begin{pmatrix} 0 \\ -\mathrm{j}\tilde{J}_{\mathrm{D}}^{(n)}(w) \end{pmatrix}. \tag{17b}$$

Hence, the choice of $\underline{\bar{\mathbf{J}}}_{\mathrm{C}}^{(n)}(\rho)$ and $\underline{\bar{\mathbf{J}}}_{\mathrm{D}}^{(n)}(\rho)$ as new unknowns allows us to deal with scalar unknowns in the spectral domain, $\tilde{J}_{\mathrm{C}}^{(n)}(w)$ and $\tilde{J}_{\mathrm{D}}^{(n)}(w)$. Such a choice will be done below.

According to the reasoning presented by Lucido et al. [23], it is possible to show that the physical behavior in (16) can be reconstructed by expanding the unknowns in the spectral domain in complete and nonredundant series of Bessel functions of the first kind [35], i.e.,

$$\tilde{J}_T^{(n)}(w) = \sum_{h=-1+\delta_{n,0}}^{+\infty} \gamma_{T,h}^{(n)} \tilde{f}_{T,h}^{(n)}(w) \tag{18}$$

where $\delta_{n,m}$ is the Kronecker delta function

$$\gamma_{\mathrm{D},-1}^{(n)} = \alpha^{(n)} \gamma_{\mathrm{C},-1}^{(n)} \tag{19a}$$

$$\alpha^{(n)} = \mathrm{j} \frac{\mathrm{sgn}(n)\,|n|!}{\Gamma\left(|n| + 1/2\right)} \sqrt{\frac{2\left(|n| - 1/2\right)}{a\,|n|}} \tag{19b}$$

$\mathrm{sgn}(\cdot)$ and $\Gamma(\cdot)$ are, respectively, the Signum function and the Gamma function [28], and

$$\tilde{f}_{T,h}^{(n)}(w) = \sqrt{2\eta_{T,h}^{(n)}} \frac{J_{\eta_{T,h}^{(n)}}(aw)}{w^{p_T}} \tag{20a}$$

$$\eta_{T,h}^{(n)} = |n| + 2h + p_T + 1 \tag{20b}$$

such that the following orthonormality property can be readily established [30]:

$$\begin{aligned} &\int_0^{+\infty} \tilde{f}_{T,k}^{(n)}(w)\, \tilde{f}_{T,h}^{(n)}(w)\, w^{2p_T - 1} dw \\ &\quad = 2\sqrt{\eta_{T,k}^{(n)} \eta_{T,h}^{(n)}} \int_0^{+\infty} \frac{1}{w} J_{\eta_{T,k}^{(n)}}(aw)\, J_{\eta_{T,h}^{(n)}}(aw)\, dw \\ &\quad = \delta_{h,k} \end{aligned} \tag{21}$$

with $h, k = -1 + \delta_{n,0}, \ldots, +\infty$.

Hence, by using the expansions (18) in a Galerkin scheme and observing that the convolution integrals resulting from the Galerkin projection reduce to algebraic products in the spectral domain, the dual integral equations (13) are recast as the following linear system of algebraic equations:

$$\begin{aligned} &\sum_{h=-1+\delta_{n,0}}^{+\infty} \gamma_{T,h}^{(n)} \int_0^{+\infty} \frac{\tilde{f}_{T,k}^{(n)}(w)\, \tilde{f}_{T,h}^{(n)}(w)}{\tilde{G}_T(w) - R} w dw \\ &\qquad = -\mathrm{j}^{n+1} e^{-\mathrm{j}n\phi_0} E_{0t} \frac{\tilde{f}_{T,k}^{(n)}\left(k_0 s_{\theta_0}\right)}{\tilde{G}_T\left(k_0 s_{\theta_0}\right) - R} \end{aligned} \tag{22}$$

with $k = -1 + \delta_{n,0}, \ldots + \infty$, where $t = \rho, \phi$ for $T = \mathrm{C}, \mathrm{D}$, respectively.

Remembering (15), (19a), and (21), by means of simple algebraic manipulations, the matrix equation (22) can be rewritten as follows:

$$\mathbf{x}^{(n)} + \mathbf{A}^{(n)} \mathbf{x}^{(n)} = \mathbf{c}^{(n)} \tag{23}$$

where the vector of the unknown coefficients, $\mathbf{x}^{(n)}$, the coefficient matrix, $\mathbf{A}^{(n)}$, and the free-term vector, $\mathbf{c}^{(n)}$, are specified in Appendix C.

By adopting the technique developed in [23], it is possible to demonstrate that, even in such a case, Galerkin projection acts as a perfect preconditioner and the obtained matrix equation (23) is of the Fredholm second-kind in l^2, i.e., the existence of the solution arises from the uniqueness and the solution of the truncated matrix equation converges to the exact solution of the infinite algebraic problem as the truncation order tends to infinity. Moreover, as will be shown in Section III, since the expansion functions reconstruct the physical behavior of the unknowns, few of them are needed to achieve reasonably accurate solutions, thus leading to a small-size coefficient matrix. On the other hand, by using the analytical procedure introduced by Lucido et al. [22] and [23], the elements of the coefficient matrix, which are 1-D improper integrals of oscillating and slowly decaying functions, are alternatively written as linear combinations of fast converging proper integrals efficiently numerically evaluated by means of an in-house software code implementing an adaptive Gauss-Legendre quadrature routine in C++ environment [36].

C. Near-Field and Far-Field Reconstruction

Once $\underline{\tilde{\mathbf{J}}}^{(n)}(\rho)$ is found, the VHT_n of the nth azimuthal harmonic of the effective electric surface current density can be immediately obtained

$$\underline{\tilde{\mathbf{J}}}^{(n)}(w) = \left(\underline{\underline{\tilde{\mathbf{G}}}}(w) - R\underline{\underline{\mathbf{I}}}\right)^{-1} \left(\underline{\tilde{\mathbf{J}}}^{(n)}(w) - \underline{\tilde{\mathbf{E}}}_t^{\mathrm{inc}(n)}(w, 0)\right) \tag{24}$$

and the nth azimuthal harmonic of the electric field scattered by the holed resistive plane reconstructed by means of (6). On the other hand, even the nth azimuthal harmonic of the electric field scattered by the resistive plane without hole can be reconstructed by using (6) as long as $\underline{\tilde{\mathbf{J}}}^{(n)}(w)$ is replaced by

$$\underline{\tilde{\mathbf{J}}}_0^{(n)}(w) = -\left(\underline{\underline{\tilde{\mathbf{G}}}}\left(k_0 s_{\theta_0}\right) - R\underline{\underline{\mathbf{I}}}\right)^{-1} \underline{\tilde{\mathbf{E}}}_t^{\mathrm{inc}(n)}(w, 0) \tag{25}$$

which is the VHT_n of the nth azimuthal harmonic of the effective electric surface current density on the resistive plane without hole (see Appendix B). Hence, by the definitions of diffracted and scattered fields, it is simple to conclude that the nth azimuthal harmonic of the electric field diffracted by the holed resistive plane coincides with the scattered electric field generated by $\underline{\tilde{\mathbf{J}}}^{(n)}(w) - \underline{\tilde{\mathbf{J}}}_0^{(n)}(w)$, i.e.,

$$\begin{aligned} &\underline{\mathbf{E}}_t^{\mathrm{diffr}(n)}(\rho, z) \\ &\quad = \int_0^{+\infty} \underline{\underline{\mathbf{H}}}^{(n)}(w\rho)\, \underline{\underline{\tilde{\mathbf{G}}}}(w) \left(\underline{\tilde{\mathbf{J}}}^{(n)}(w) - \underline{\tilde{\mathbf{J}}}_0^{(n)}(w)\right) \\ &\qquad \cdot e^{-\mathrm{j}\sqrt{k_0^2 - w^2}|z|} w dw \end{aligned}$$

$$= \int_0^{+\infty} \underline{\underline{\mathbf{H}}}^{(n)}(w\rho)\,\underline{\underline{\tilde{\mathbf{G}}}}(w)\left(\underline{\underline{\tilde{\mathbf{G}}}}(w) - R\underline{\underline{\mathbf{I}}}\right)^{-1}\underline{\tilde{\tilde{\mathbf{J}}}}^{(n)}(w) \cdot e^{-\mathrm{j}\sqrt{k_0^2-w^2}|z|}\,w\,dw \tag{26a}$$

$$E_z^{\mathrm{diffr}(n)}(\rho,z) = -\mathrm{j}\frac{\mathrm{sgn}(z)}{2\omega\varepsilon_0}\int_0^{+\infty} J_n(w\rho)\left(\tilde{J}_{\mathrm{C}}^{(n)}(w) - \tilde{J}_{0,\mathrm{C}}^{(n)}(w)\right) \cdot e^{-\mathrm{j}\sqrt{k_0^2-w^2}|z|}\,w^2\,dw = -\mathrm{j}\frac{\mathrm{sgn}(z)}{2\omega\varepsilon_0}\int_0^{+\infty} J_n(w\rho)\left(\tilde{G}_{\mathrm{C}}(w) - R\right)^{-1}\tilde{\tilde{J}}_{\mathrm{C}}^{(n)}(w) \cdot e^{-\mathrm{j}\sqrt{k_0^2-w^2}|z|}\,w^2\,dw \tag{26b}$$

where (6), (11), (24), and (25) have been used.

Note that the kernels in (26) have no real-valued poles if the resistivity R is real (see Appendix A). Then, by means of the stationary phase method, the far-diffracted electric field can be expressed in closed form as

$$E_s^{\mathrm{diffr}}(\underline{r}) \overset{r\to\infty}{\sim} \frac{e^{-jk_0r}}{r}F_s(\theta,\phi) \tag{27}$$

for $s = \theta, \phi$, where

$$F_\theta(\theta,\phi) = -\frac{\omega\mu_0}{2}c_\theta\left(\tilde{G}_{\mathrm{C}}(k_0s_\theta) - R\right)^{-1} \times \sum_{n=-\infty}^{+\infty} e^{jn\left(\phi+\frac{\pi}{2}\right)}\tilde{\tilde{J}}_{\mathrm{C}}^{(n)}(k_0s_\theta) \tag{28a}$$

$$F_\phi(\theta,\phi) = -\frac{\omega\mu_0}{2}\left(\tilde{G}_{\mathrm{D}}(k_0s_\theta) - R\right)^{-1} \times \sum_{n=-\infty}^{+\infty} e^{jn\left(\phi+\frac{\pi}{2}\right)}\tilde{\tilde{J}}_{\mathrm{D}}^{(n)}(k_0s_\theta) \tag{28b}$$

and the bistatic radar cross section (BRCS) and the total scattering cross section (TSCS), defined by the diffracted field, can be expressed as

$$\sigma_{\mathrm{BRCS}}(\theta,\phi) = \lim_{r\to\infty}\frac{4\pi r^2\left|\underline{E}^{\mathrm{diffr}}(\underline{r})\right|^2}{\left|\underline{E}^{\mathrm{inc}}(\underline{r})\right|^2} = \frac{4\pi\left|\underline{F}(\theta,\phi)\right|^2}{\left|\underline{E}_0\right|^2} \tag{29a}$$

$$\sigma_{\mathrm{TSCS}} = \frac{1}{4\pi}\int_0^{\pi}\int_0^{2\pi}\sigma_{\mathrm{BRCS}}(\theta,\phi)\,s_\theta\,d\phi\,d\theta = \frac{1}{\left|\underline{E}_0\right|^2}\int_0^{\pi}\int_0^{2\pi}\left|\underline{F}(\theta,\phi)\right|^2 s_\theta\,d\phi\,d\theta. \tag{29b}$$

III. Numerical Results

This section is devoted to the demonstration of the fast convergence of the proposed technique in reconstructing near-field and far-field characteristics for the problem at hand, for varying values of the radius of the hole, the resistivity of the holed plane, the incidence angle, and the polarization of the impinging plane wave.

In order to examine the convergence rate of the proposed method, the following relative computation error is introduced:

$$err_N(M) = \sqrt{\frac{\sum_{n=-N+1}^{N-1}\left\|\mathbf{x}_{M+1}^{(n)} - \mathbf{x}_M^{(n)}\right\|^2}{\sum_{n=-N+1}^{N-1}\left\|\mathbf{x}_M^{(n)}\right\|^2}} \tag{30}$$

where the symbol $\|\cdot\|$ denotes the usual Euclidean norm, $\mathbf{x}_M^{(n)}$ is the truncated vector of the expansion coefficients, M is the number of expansion functions used for each unknown, whereas $2N-1$ harmonics are considered according to the estimation formula proposed in [37]. It is remarkable to note that, by exploiting all the symmetries of the coefficient matrix, just $NM(2M+1)$ of $4M^2(2N-1)$ matrix elements have to be numerically evaluated.

Moreover, comparisons with the results provided by CST-MWS are presented to validate the implemented software code and to show that the proposed method drastically outperforms CST-MWS in terms of computation time and memory occupation. To this purpose, all the simulations are performed on a laptop equipped with an Intel Core i7-10510U 1.8 GHz, 16 GB RAM.

In Fig. 2, the problem for $a = 2\lambda$, $R = 1$ kΩ, and TE incidence with $\phi_0 = 0°$ and $\theta_0 = 0°, 30°, 60°$ is analyzed. In Fig. 2(a), the relative computation error is shown. As can be clearly seen, the asymptotic convergence is substantially independent of the incidence angle, which instead affects the number of azimuthal harmonics to be considered ($N = 2, 15, 21$, respectively). As expected, the convergence is really very fast as at most seven expansion functions for each unknown and a computation time of at most 2 s are needed to achieve a relative computation error of 1%, whereas 13 expansion functions and 4 s allow achieving an error of 0.1%. In Fig. 2(b), the amplitude of the auxiliary unknown along the direction $\theta = 90°$ and $\phi = 0°, 180°$ is plotted. According to (15), the auxiliary unknown assumes constant values at the hole rim because its ρ-component vanishes. Fig. 2(c) shows the BRCS in the plane $\phi = 0°, 180°$. As expected, two maxima substantially directed along the specular with respect to the incidence direction and the forward direction appear.

Fig. 3 is related to the second case analyzed: $a = \lambda, 2\lambda, 4\lambda$, $R = 1$ kΩ and TM incidence with $\phi_0 = 0°$ and $\theta_0 = 30°$. The relative computation error is plotted in Fig. 3(a). In this case, the numbers of both the expansion functions and the azimuthal harmonics, needed to achieve a given accuracy, increase if the hole radius gets larger. Anyway, the convergence is really very fast in all the cases examined. Indeed, $N = 11, 15, 23$ has to be set for $a = \lambda, 2\lambda, 4\lambda$, respectively. Moreover, at most $M = 8$ and a computation time of 3 s are needed to achieve a relative computation error of less than 1%, whereas at most $M = 16$ and 8 s allow to reach a relative computation error of less than 0.1%. It is important to note that the fast convergence for varying values of the radius of the hole with respect to the wavelength can be immediately reinterpreted as the effectiveness of the proposed full-wave method for varying values of the frequency. Fig. 3(b) shows the amplitude of the auxiliary unknown along the direction $\theta = 90°$ and

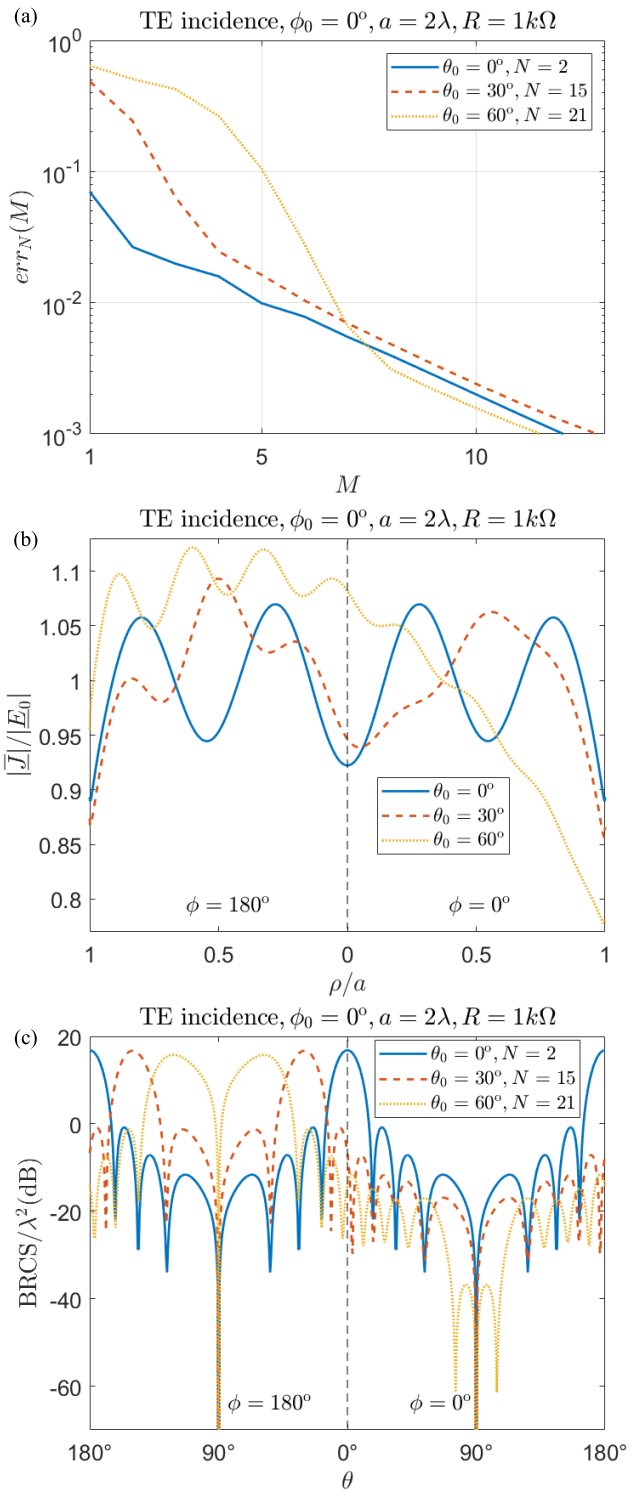

Fig. 2. (a) Relative computation error, (b) amplitude of the auxiliary function along the direction $\theta = 90°$ and $\phi = 0°, 180°$, and (c) normalized BRCS in the plane $\phi = 0°, 180°$ for the holed resistive plane with $a = 2\lambda$, $R = 1$ kΩ and TE incidence with $\phi_0 = 0°$ and $\theta_0 = 0°, 30°, 60°$.

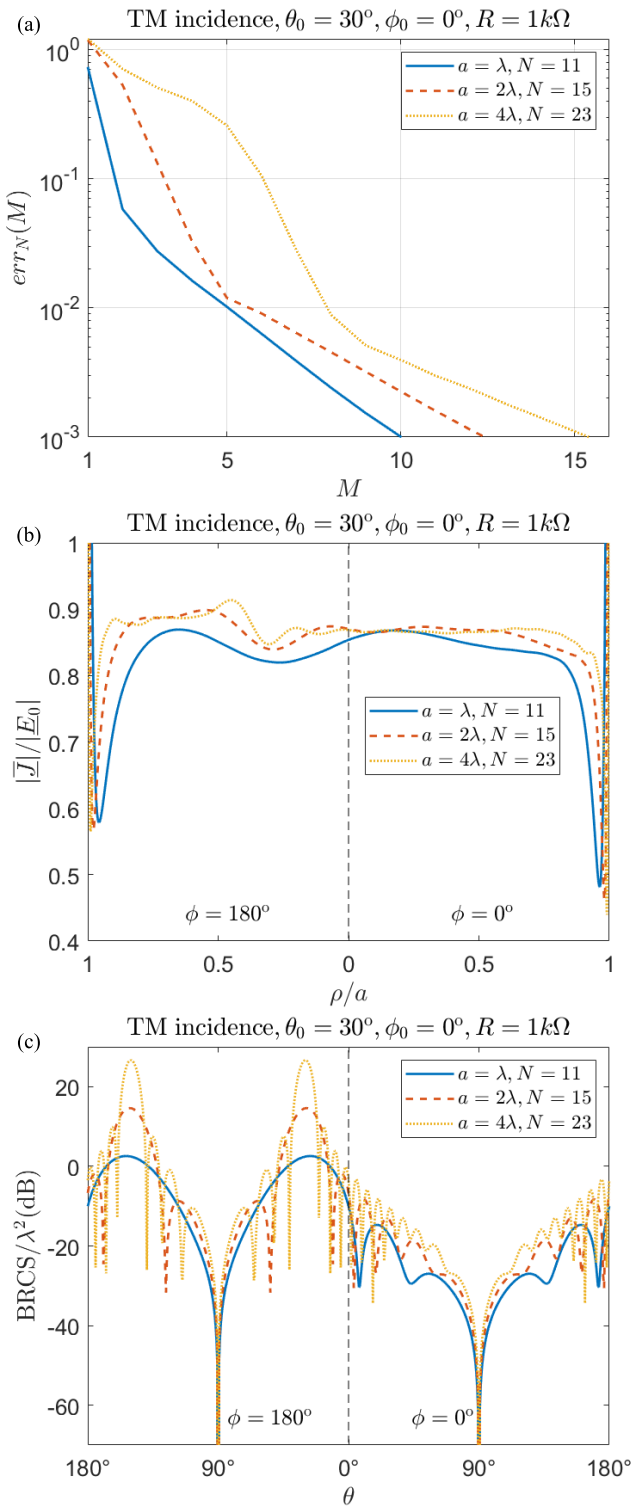

Fig. 3. (a) Relative computation error, (b) amplitude of the auxiliary function along the direction $\theta = 90°$ and $\phi = 0°, 180°$, and (c) normalized BRCS in the plane $\phi = 0°, 180°$ for the holed resistive plane with $a = \lambda, 2\lambda, 4\lambda$, $R = 1$ kΩ and TM incidence with $\phi_0 = 0°$ and $\theta_0 = 30°$.

$\phi = 0°, 180°$. In that case, the ρ-component of the auxiliary unknown does not vanish, and a divergent behavior can be observed at the hole rim [see (16)]. As expected, the BRCS behavior in the plane $\phi = 0°, 180°$ plotted in Fig. 3(c) shows that the number of sidelobes increases by increasing the radius of the hole.

In Fig. 4, the case of $a = 2\lambda$, $R = 0.1, 1, 10$ kΩ and TE incidence with $\phi_0 = 0°$ and $\theta_0 = 30°$ is considered. Fig. 4(a) shows the behavior of the relative computation error. Of course, the resistivity level does not affect the number of azimuthal harmonics to be considered ($N = 15$ in that case). However, it has an impact on the number of expansion

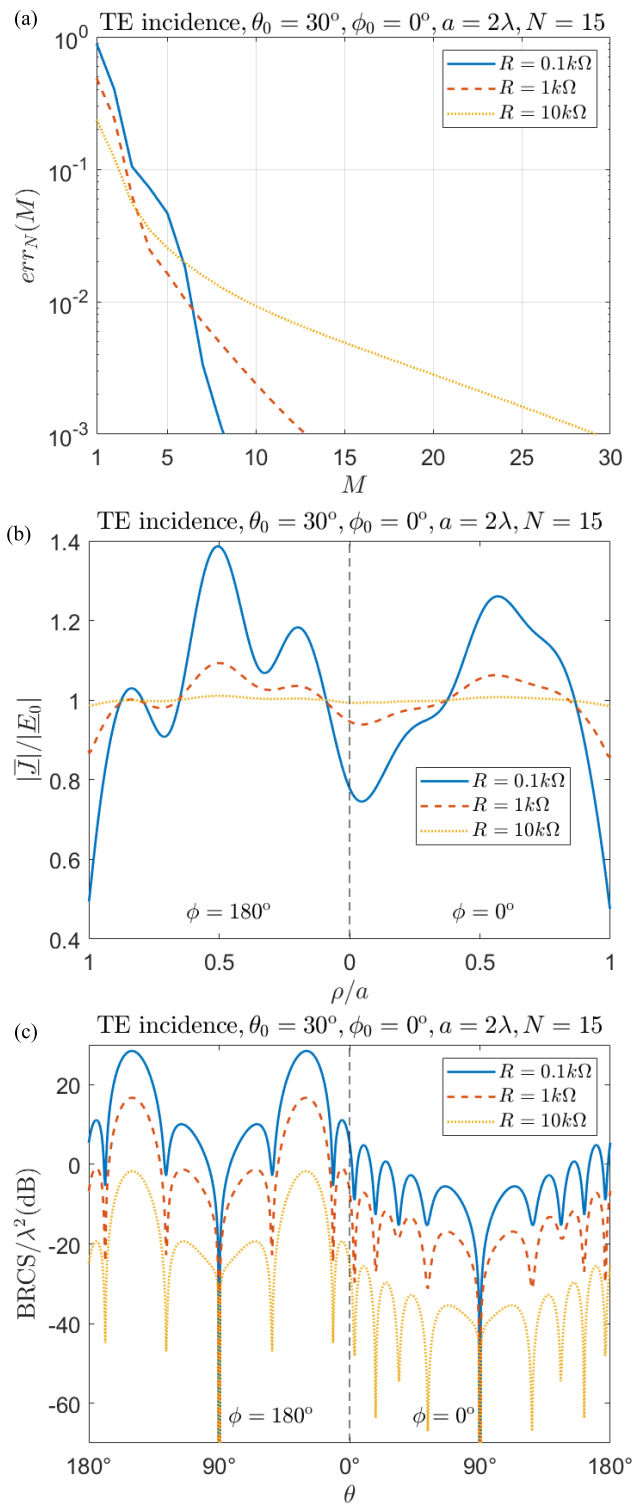

Fig. 4. (a) Relative computation error, (b) amplitude of the auxiliary function along the direction $\theta = 90°$ and $\phi = 0°, 180°$, and (c) normalized BRCS in the plane $\phi = 0°, 180°$ for the holed resistive plane with $a = 2\lambda$, $R = 0.1, 1, 10$ kΩ and TE incidence with $\phi_0 = 0°$ and $\theta_0 = 30°$.

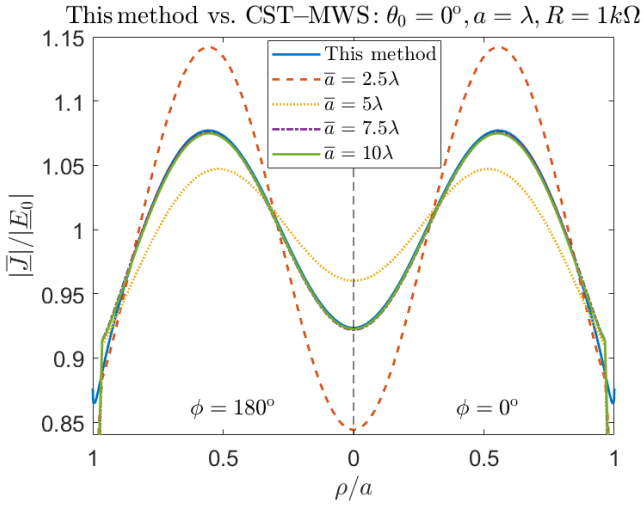

Fig. 5. Amplitude of the auxiliary function along the direction $\theta = 90°$ and $\phi = 0°, 180°$ for the holed resistive plane with $a = \lambda$, $R = 1$ kΩ, and normal incidence ($\theta_0 = 0°$) with the electric field along the direction $\theta = 90°$ and $\phi = 90°, 270°$, reconstructed by means of the presented method, and using CST-MWS by approximating the holed resistive plane with a zero-thickness resistive annular ring of internal radius a and external radius $\bar{a}$ for $\bar{a} = 2.5\lambda, 5\lambda, 7.5\lambda, 10\lambda$.

functions to be used as higher is the accuracy required for the solution, although the convergence is in any case very fast. Indeed, in the three cases examined in this example, a relative computation error of 1% is achieved by using from 6 to 9 expansion functions for each unknown with a computation time of about 3 s, whereas an error of 0.1% requires from 9 to 30 expansion functions with a computation time ranging from 2 to 15 s. Fig. 4(b) shows the amplitude of the auxiliary unknown along the direction $\theta = 90°$ and $\phi = 0°, 180°$. It is interesting to note that such behavior tends to the amplitude of the incident field for increasing values of the resistivity, i.e., the scattered field tends to vanish, coherently with the total transparency expected when the resistivity tends to infinity. This conclusion is confirmed by the BRCS behavior in the plane $\phi = 0°, 180°$ plotted in Fig. 4(c), which shows a reduction in all the directions by increasing the resistivity level.

Comparisons with CST-MWS are provided in order to validate the implemented in-house software code and to show the effectiveness of the proposed method. The integral equation solver of CST-MWS combined with the zero-thickness representation of the scatterer has been considered. Obviously, CST-MWS is not able to simulate the considered in finite object, hence, the holed resistive plane has been approximated with a zero-thickness resistive annular ring of internal radius a and external radius $\bar{a}$. In Fig. 5, the amplitude of the auxiliary function along the direction $\theta = 90°$ and $\phi = 0°, 180°$ for $a = \lambda$, $R = 1$ kΩ, $\theta_0 = 0°$ (normal incidence), and incident electric field along the direction $\theta = 90°$ and $\phi = 90°, 270°$, reconstructed by using ten expansion functions and two azimuthal harmonics (for $n = \pm 1$), i.e., 800 matrix coefficients, in order to achieve a relative computation error less than 0.1% with a computation time of 1.5 s, is compared with the behavior obtained by using CST-MWS for four values of the external radius ($\bar{a} = 2.5\lambda, 5\lambda, 7.5\lambda, 10\lambda$). It is clear that the solution provided by CST-MWS tends to be the one obtained by means of the proposed method as the external radius increases. In the very simple case examined, a quite good approximation is obtained by considering at least $\bar{a} = 7.5\lambda$. However, it is possible to show that higher values of $\bar{a}$ have to be used for

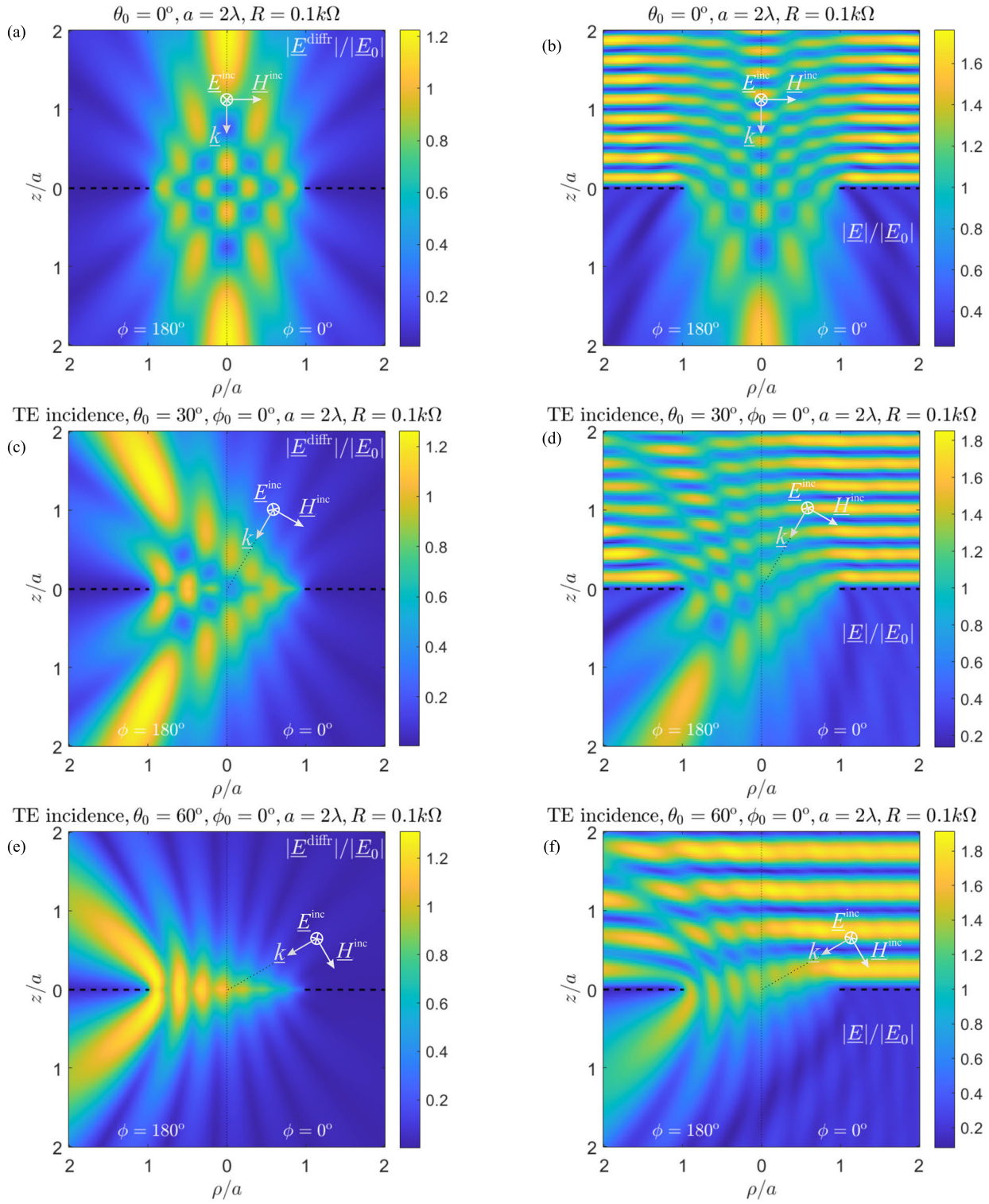

Fig. 6. Diffracted and total near electric fields in the plane $\phi = 0°, 180°$ for $a = 2\lambda$, $R = 0.1$ kΩ and TE incidence with $\phi_0 = 0°$ and $\theta_0 = 0°, 30°, 60°$. (a) Diffracted near electric field for $\theta_0 = 0°$, (b) total near electric field for $\theta_0 = 0°$, (c) diffracted near electric field for $\theta_0 = 30°$, (d) total near electric field for $\theta_0 = 30°$, (e) diffracted near electric field for $\theta_0 = 60°$, and (f) total near electric field for $\theta_0 = 60°$.

increasing values of a and/or θ_0. In Table I, the number of mesh cells and the corresponding computation times needed to reconstruct the solution by means of CST-MWS for all the cases examined in Fig. 5 are shown and compared with the proposed method. As can be seen, 0.6 to 9.3 million mesh cells have been used and the required computation time varies from 90 to 542 s. The obvious conclusion is that the proposed method drastically outperforms CST-MWS. As, in contrast to CST-MWS, our technique possesses a mathematically guaranteed convergence, it is fair to view the found agreements as a validation of the former and not the latter.

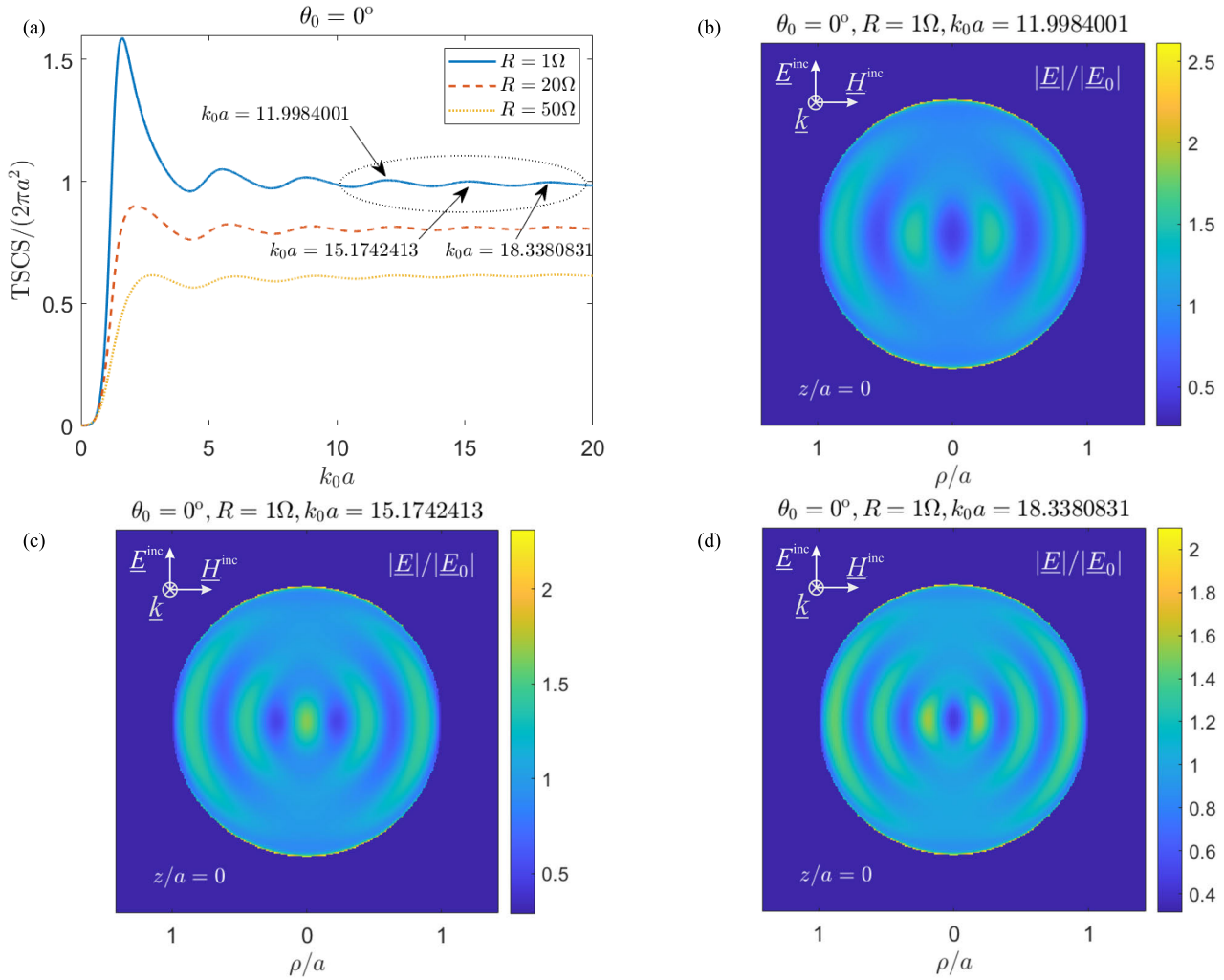

Fig. 7. Normalized TSCS for varying values of the normalized frequency (k_0a) and $R = 1, 20, 50\ \Omega$, and total near electric field in the plane $z/a = 0$ for $R = 1\ \Omega$ at three resonance frequencies, for normal incidence ($\theta_0 = 0°$) with the electric field along the direction $\theta = 90°$ and $\phi = 90°, 270°$. (a) Normalized TSCS, (b) total near electric field at $k_0a = 11.9984001$, (c) total near electric field at $k_0a = 15.1742413$, and (d) total near electric field at $k_0a = 18.3380831$.

TABLE I

MEMORY OCCUPATION AND COMPUTATION TIME REQUIRED BY CST-MWS TO RECONSTRUCT THE AUXILIARY FUNCTION ALONG THE DIRECTION $\theta = 90°$ AND $\phi = 0°, 180°$ BY APPROXIMATING THE HOLED RESISTIVE PLANE WITH A ZERO-THICKNESS RESISTIVE ANNULAR RING OF RADII a AND $\bar{a}$ FOR $a = \lambda$, $\bar{a} = 2.5\lambda, 5\lambda, 7.5\lambda, 10\lambda$, $R = 1\ \mathrm{k}\Omega$, AND NORMAL INCIDENCE ($\theta_0 = 0°$) WITH INCIDENT ELECTRIC FIELD ALONG THE DIRECTION $\theta = 90°$ AND $\phi = 90°, 270°$, AND COMPARISON WITH THE PROPOSED METHOD

CST-MWS	NUMBER OF MESH-CELLS	COMPUTATION TIME (SECONDS)
$\bar{a} = 2.5\lambda$	600000	90
$\bar{a} = 5\lambda$	2400000	206
$\bar{a} = 7.5\lambda$	5300000	346
$\bar{a} = 10\lambda$	9300000	542
THIS METHOD	NUMBER OF MATRIX COEFFICIENTS	COMPUTATION TIME (SECONDS)
	800	1.5

For the sake of completeness, in Fig. 6, the diffracted and total near electric fields in the plane $\phi = 0°, 180°$ are shown for $a = 2\lambda$, $R = 0.1\ \mathrm{k}\Omega$ and TE incidence with $\phi_0 = 0°$ and $\theta_0 = 0°, 30°, 60°$. As expected, the amplitude of the diffracted field is symmetric with respect to the holed resistive plane and the hotspots are substantially directed along the specular with respect to the incidence direction and the forward direction. On the other hand, the total field behavior clearly shows the interference between the incidence and reflected waves, and the perturbation of the field due to the diffraction phenomenon.

To conclude, the natural mode resonances of the holed resistive plane are analyzed. For the sake of brevity, the following discussion is limited to the normal incidence of the plane wave ($\theta_0 = 0°$). As a result, only the harmonics $n = \pm 1$ contribute to the field representation.

According to [20], the resonance frequencies can be individuated by the peaks of TSCS. In Fig. 7(a), the TSCS is plotted for varying values of the normalized frequency, k_0a, and for $R = 1, 20, 50\ \Omega$. This behavior has been reconstructed by using from 4 to 35 expansion functions in order to achieve a relative computation error of less than 0.1% for each simulation point with a computation time ranging from 0.4 to 5 s. It can be immediately observed

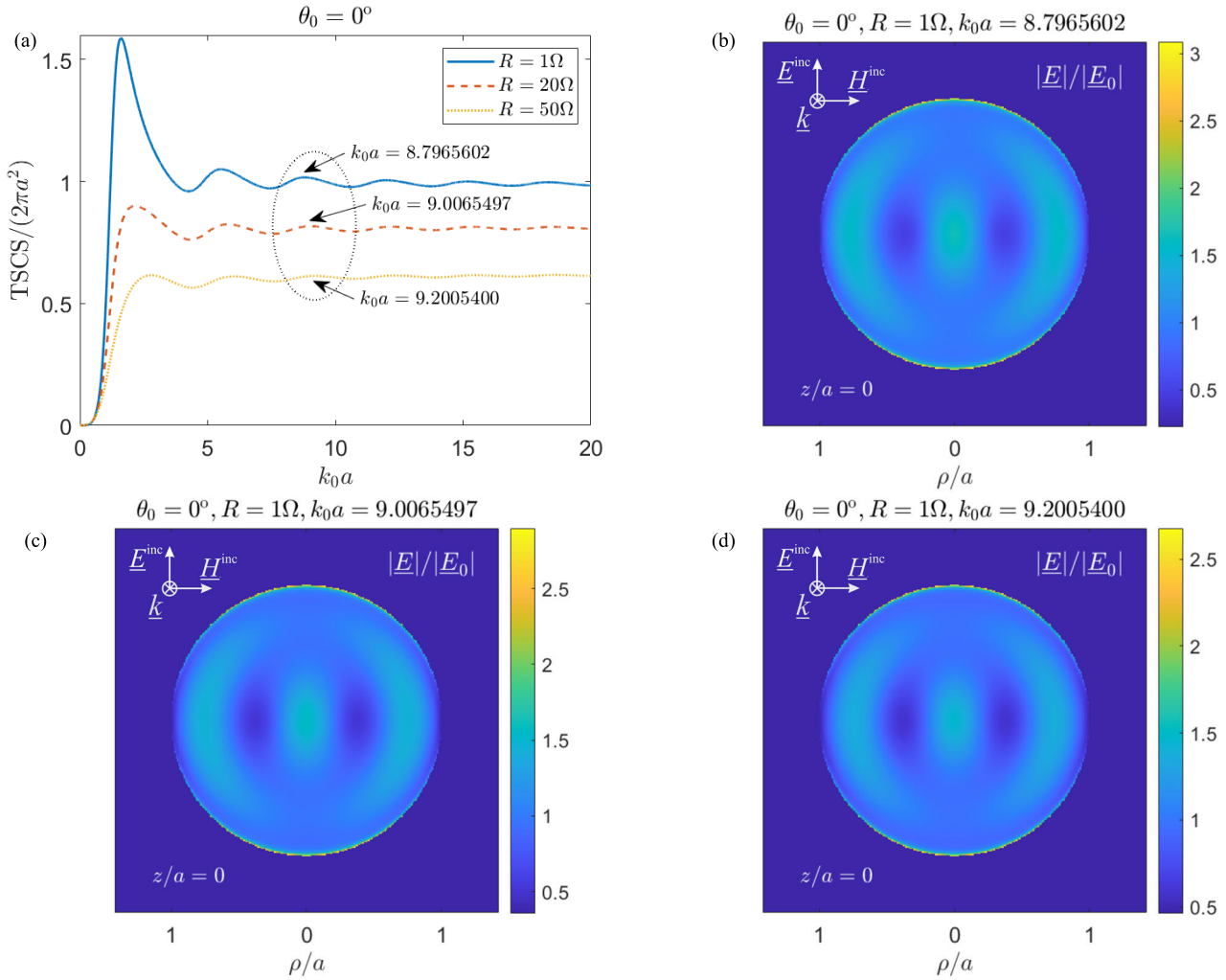

Fig. 8. Normalized TSCS for varying values of the normalized frequency (k_0a) and total near electric field in the plane $z/a = 0$ for one natural mode resonance, for $R = 1, 20, 50$ and normal incidence ($\theta_0 = 0°$) with the electric field along the direction $\theta = 90°$ and $\phi = 90°, 270°$. (a) Normalized TSCS, (b) total near electric field for $R = 1\ \Omega$ and $k_0a = 8.7965602$, (c) total near electric field for $R = 20\ \Omega$ and $k_0a = 9.0065497$, and (d) total near electric field for $R = 50\ \Omega$ and $k_0a = 9.2005400$.

that, coherently with the BRCS behavior shown in Fig. 4(c), the TSCS reduces as the resistivity increases, i.e., by moving toward the total transparency condition. Moreover, many peaks can be observed in all the cases examined that are as smoother out as the surface resistivity is higher. This behavior can be directly connected to lower values of the associated resonance quality factors. In Fig. 7(b)–(d), the in-plane ($z/a = 0$) total electric field behavior at the three consecutive resonance frequencies $k_0a = 11.9984001$, $k_0a = 15.1742413$, and $k_0a = 18.3380831$, marked in Fig. 7(a), is shown. Such kinds of resonances, with an azimuthal index $n = 1$, are commonly called dipole-mode resonances [20] and show the hotspots stretched only along the incidence magnetic field direction. As expected, the number of hotspots increases by increasing the resonance frequency. Moreover, a bright edge can be observed at the hole rim due to the field singularity [31], and the field substantially vanishes outside the hole in the hole plane.

In Fig. 8(a), the same TSCS behavior as in Fig. 7(a) is plotted, however, the normalized resonance frequencies of the same natural mode resonance for different values of the resistivity, i.e., $k_0a = 8.7965602$ for $R = 1\ \Omega$, $k_0a = 9.0065497$ for $R = 20\ \Omega$, and $k_0a = 9.2005400$ for $R = 50\ \Omega$, are marked, whereas the corresponding in-plane total electric field behavior is shown in Fig. 8(b)–(d). As can be seen, Fig. 8(b)–(d) are substantially indistinguishable. This demonstrates that the resonance frequencies can be tuned by acting on the resistivity level. This very interesting property is particularly attractive when dealing with materials like graphene for which the resistivity level can be simply tuned with the aid of a DC bias.

IV. Conclusion

The plane wave diffraction from a circular hole in an infinite resistive plane has been carried out by means of the generalized boundary condition and a guaranteed and fast convergence semi-analytical technique. The proposed formulation overcomes the need of dealing with unknowns defined on an infinite support and includes the PEC case as a limit case. The accuracy and efficiency of the proposed technique have been demonstrated by the numerous results provided and the

comparisons with CST-MWS. It is worth observing that the accurate analysis of the absorption characteristics and of the surface wave propagation (in the case of complex R) can be readily performed with the proposed method and will be the subject of future papers. Moreover, the proposed method is fully applicable to the analysis of a holed graphene plane and can be readily generalized to study a thin holed dielectric plate. Future perspectives are the generalization of the proposed method to analyze the diffraction from arrays of circular holes in resistive planes and holed planes in layered media.

APPENDIX A

Let us consider the infinite material plate shown in Fig. 1(a) assuming that there is no hole, i.e., $a = 0$.

Supposing that $\sigma \gg \omega\varepsilon_0\varepsilon_r$ and $\tau < d_{skin} \ll \lambda$, the plate can be approximated with a zero-thickness resistive plane [24], located on the plate median surface S. This plane is characterized with the aid of the two-side generalized boundary conditions (1), where $R = 1/(\sigma\tau)$. Moreover, the dyadic Green's function of the 3-D space containing the infinite resistive plane can be readily obtained by means of the separation of variables and expressed in closed form in the spectral domain.

In the presence of an infinite resistive plane, to guarantee the solution uniqueness of the scattering problem associated with a finite-size scatterer, a radiation condition at infinity is needed. This condition can be established by analyzing the far-zone behavior of the corresponding Green's function, which is compliant with the principle of radiation (no field sources at infinity). Such analysis brings us to an expression similar to (43) of [38] (without the second term), i.e., the asymptotic behavior of the field diffracted by the finite-size scatterer can be expressed as the sum of a spherical wave and a guided cylindrical surface wave, if the latter exists

$$\left(\underline{E}^{\text{diffr}}\left(\underline{r}\right), \underline{H}^{\text{diffr}}\left(\underline{r}\right)\right) \overset{r\to\infty}{\sim} \left(\underline{E}^{\text{sph}}\left(\underline{r}\right), \underline{H}^{\text{sph}}\left(\underline{r}\right)\right) + \left(\underline{E}^{\text{guid}}\left(\underline{r}\right), \underline{H}^{\text{guid}}\left(\underline{r}\right)\right) \tag{A1}$$

where

$$E^{\text{sph}}_{\theta,\phi}\left(\underline{r}\right) = \pm\zeta_0 H^{\text{sph}}_{\phi,\theta}\left(\underline{r}\right) = \frac{e^{-jk_0 r}}{r} F_{\theta,\phi}\left(\theta,\phi\right) \tag{A2a}$$

$$E^{\text{sph}}_{r}\left(\underline{r}\right), H^{\text{sph}}_{r}\left(\underline{r}\right) \sim o\left(\frac{1}{r}\right) \tag{A2b}$$

$$\left(\underline{E}^{\text{guid}}\left(\underline{r}\right), \underline{H}^{\text{guid}}\left(\underline{r}\right)\right) = e^{-\sqrt{w_T^2 - k_0^2}|z|} \frac{e^{-jw_T\rho}}{\sqrt{\rho}} \cdot \left(\underline{G}^E_T\left(\phi\right), \underline{G}^H_T\left(\phi\right)\right) \tag{A2c}$$

$\zeta_0 = \sqrt{\mu_0/\varepsilon_0}$ is the intrinsic impedance of the free space, $T = \text{C}, \text{D}$, $\underline{G}^{E,H}_T(\phi)$ is a suitable vector functions, whereas w_T is the propagation constant of one of two possible natural waves of different polarization, supported by the resistive plane. Such propagation constants satisfy the dispersion equations

$$\tilde{G}_T\left(w_T\right) - R = 0 \tag{A3}$$

which have explicit solutions

$$w_{\text{C}} = k_0\sqrt{1 - \left(\frac{2R}{\zeta_0}\right)^2} \tag{A4a}$$

$$w_{\text{D}} = k_0\sqrt{1 - \left(\frac{\zeta_0}{2R}\right)^2}. \tag{A4b}$$

Note that $w = w_{\text{C}}$ and $w = w_{\text{D}}$ are also the poles, complex in the general case, of the integrand in (13a).

The natural waves of the resistive plane are the residues in these poles. As one can see, these natural waves are *guided waves* with purely real propagation constants larger than k_0, i.e., they take power to infinity (at $\rho \to \infty$), only if R is purely imaginary and either $\text{Im}R < 0$ for w_{C} or $\text{Im}R > 0$ for w_{D}. In the case considered in this article, when R is purely real, either of these natural waves decays exponentially at infinity, hence the second term in (A1) can be safely neglected. This leaves us with the first term, which is a spherical wave satisfying the usual Silver-Muller radiation condition. As known from [39], the asymptotic form of that condition, given by (A2a) and (A2b), is equivalent to the differential form, $\lim_{r\to\infty} r(\underline{E}^{\text{diffr}}(\underline{r}) - \zeta_0 \underline{H}^{\text{diffr}}(\underline{r}) \times \hat{r}) = \underline{0}\cdot\hat{\theta}$.

APPENDIX B

In the case of plane-wave scattering from the uniform resistive plane discussed in Appendix A, the diffracted field vanishes. Hence, in the half-space above the plane, the total field is the superposition of the incident and the reflected plane waves, whereas, in the half-space below, the field is given by the transmitted plane wave.

Then, the tangential to the resistive plane components of the incident/reflected/transmitted field for the TM/TE (with respect to the z axis) polarization of the impinging plane wave can be readily derived in explicit form as follows:

$$\underline{E}^{\text{refl}}_{t,P}\left(\rho,\phi,0^+\right) = \Gamma^P \underline{E}^{\text{inc}}_{t,P}\left(\rho,\phi,0\right) \tag{B1a}$$

$$\underline{E}^{\text{tr}}_{t,P}\left(\rho,\phi,0^-\right) = \tau^P \underline{E}^{\text{inc}}_{t,P}\left(\rho,\phi,0\right) \tag{B1b}$$

$$\hat{z} \times \underline{H}^{\text{inc}}_{P}\left(\rho,\phi,0\right) = \frac{1}{Z^P_0} \underline{E}^{\text{inc}}_{t,P}\left(\rho,\phi,0\right) \tag{B1c}$$

$$\hat{z} \times \underline{H}^{\text{refl}}_{P}\left(\rho,\phi,0^+\right) = -\frac{\Gamma^P}{Z^P_0} \underline{E}^{\text{inc}}_{t,P}\left(\rho,\phi,0\right) \tag{B1d}$$

$$\hat{z} \times \underline{H}^{\text{tr}}_{P}\left(\rho,\phi,0^-\right) = \frac{\tau^P}{Z^P_0} \underline{E}^{\text{inc}}_{t,P}\left(\rho,\phi,0\right) \tag{B1e}$$

with $P = \text{TM}, \text{TE}$, where

$$\Gamma^P = -\frac{Z^P_0}{Z^P_0 + 2R} \tag{B2a}$$

$$\tau^P = 1 + \Gamma^P \tag{B2b}$$

are the reflection and transmission coefficients, respectively, and

$$Z^{\text{TM}}_0 = \zeta_0 c_{\theta_0} = -2\tilde{G}_{\text{C}}\left(k_0 s_{\theta_0}\right) \tag{B3a}$$

$$Z^{\text{TE}}_0 = \frac{\zeta_0}{c_{\theta_0}} = -2\tilde{G}_{\text{D}}\left(k_0 s_{\theta_0}\right). \tag{B3b}$$

Moreover, the jump across the resistive plane of the tangential component of the magnetic field defines the following effective electric surface current density:

$$\begin{aligned}\underline{J}_0^P(\rho,\phi) &= \hat{z}\times\left(\underline{H}_P(\rho,\phi,0^+)-\underline{H}_P(\rho,\phi,0^-)\right)\\ &= \hat{z}\times\Big(\underline{H}_P^{\text{inc}}(\rho,\phi,0)+\underline{H}_P^{\text{refl}}(\rho,\phi,0^+)\\ &\qquad -\underline{H}_P^{\text{tr}}(\rho,\phi,0^-)\Big)\\ &= -\frac{2\Gamma^P}{Z_0^P}\underline{E}_{t,P}^{\text{inc}}(\rho,\phi,0)\end{aligned}\tag{B4}$$

where the relations (B1c)–(B1e) have been used.

It is well-known that a generally polarized incident plane wave can be written as the superposition of a TM and a TE polarized plane waves. Hence, due to the linearity, by means of the superposition principle, the effective electric surface current density and the tangential component of the transmitted electric field on the resistive plane can be written as follows:

$$\begin{aligned}\underline{J}_0(\rho,\phi) &= \underline{J}_0^{\text{TM}}(\rho,\phi)+\underline{J}_0^{\text{TE}}(\rho,\phi)\\ &= -\frac{2\Gamma^{\text{TM}}}{Z_0^{\text{TM}}}\underline{E}_{t,\text{TM}}^{\text{inc}}(\rho,\phi,0)\\ &\quad -\frac{2\Gamma^{\text{TE}}}{Z_0^{\text{TE}}}\underline{E}_{t,\text{TE}}^{\text{inc}}(\rho,\phi,0)\end{aligned}\tag{B5a}$$

$$\begin{aligned}\underline{E}_t^{\text{tr}}(\rho,\phi,0^-) &= \underline{E}_{t,\text{TM}}^{\text{tr}}(\rho,\phi,0^-)+\underline{E}_{t,\text{TE}}^{\text{tr}}(\rho,\phi,0^-)\\ &= \tau^{\text{TM}}\underline{E}_{t,\text{TM}}^{\text{inc}}(\rho,\phi,0)+\tau^{\text{TE}}\underline{E}_{t,\text{TE}}^{\text{inc}}(\rho,\phi,0).\end{aligned}\tag{B5b}$$

Therefore, the nth azimuthal harmonic of the corresponding Fourier series expansions are

$$\underline{\mathbf{J}}_0^{(n)}(\rho) = -\frac{2\Gamma^{\text{TM}}}{Z_0^{\text{TM}}}\underline{\mathbf{E}}_{t,\text{TM}}^{\text{inc}(n)}(\rho,0)-\frac{2\Gamma^{\text{TE}}}{Z_0^{\text{TE}}}\underline{\mathbf{E}}_{t,\text{TE}}^{\text{inc}(n)}(\rho,0)\tag{B6a}$$

$$\underline{\mathbf{E}}_t^{tr(n)}(\rho,0^-) = \tau^{\text{TM}}\underline{\mathbf{E}}_{t,\text{TM}}^{\text{inc}(n)}(\rho,0)+\tau^{\text{TE}}\underline{\mathbf{E}}_{t,\text{TE}}^{\text{inc}(n)}(\rho,0).\tag{B6b}$$

Observing that $\nabla_t\times\underline{E}_{t,\text{TM}}^{\text{inc}}(\rho,\phi,0)=0$ and $\nabla_t\cdot\underline{E}_{t,\text{TE}}^{\text{inc}}(\rho,\phi,0)=0$, and according to (17), the VHT_n of $\underline{\mathbf{J}}_0^{(n)}(\rho)$ and $\underline{\mathbf{E}}_t^{tr(n)}(\rho,0^-)$ are, respectively,

$$\begin{aligned}&\tilde{\underline{\mathbf{J}}}_0^{(n)}(w)\\ &= \begin{pmatrix}-\frac{2\Gamma^{\text{TM}}}{Z_0^{\text{TM}}}\tilde{E}_{\text{C}}^{\text{inc}(n)}(w,0)\\ 0\end{pmatrix}+\begin{pmatrix}0\\ \text{j}\frac{2\Gamma^{\text{TE}}}{Z_0^{\text{TE}}}\tilde{E}_{\text{D}}^{\text{inc}(n)}(w,0)\end{pmatrix}\\ &= -\left(\underline{\underline{\tilde{\mathbf{G}}}}(k_0 s_{\theta_0})-R\underline{\underline{\mathbf{I}}}\right)^{-1}\underline{\tilde{\mathbf{E}}}_t^{\text{inc}(n)}(w,0)\end{aligned}\tag{B7a}$$

$$\begin{aligned}&\underline{\tilde{\mathbf{E}}}_t^{\text{tr}(n)}(w,0^-)\\ &= \begin{pmatrix}\tau^{\text{TM}}\tilde{E}_{\text{C}}^{\text{inc}(n)}(w,0)\\ 0\end{pmatrix}+\begin{pmatrix}0\\ -\text{j}\tau^{\text{TE}}\tilde{E}_{\text{D}}^{\text{inc}(n)}(w,0)\end{pmatrix}\\ &= R\left(\underline{\underline{\tilde{\mathbf{G}}}}(k_0 s_{\theta_0})-R\underline{\underline{\mathbf{I}}}\right)^{-1}\underline{\tilde{\mathbf{E}}}_t^{\text{inc}(n)}(w,0).\end{aligned}\tag{B7b}$$

Moreover, by taking the VHT_n^{-1} of (B7b) and using (9), formula (14) can be immediately obtained.

APPENDIX C

In this Appendix, the matrix equation in (23) is described. The vector of the unknown coefficients is

$$\mathbf{x}^{(n)} = \begin{bmatrix}\sqrt{2\omega\varepsilon_0}\mathbf{x}_{\text{C}}^{(n)}\\ \frac{1}{\sqrt{-\text{j}R}}\mathbf{x}_{\text{D}}^{(n)}\end{bmatrix}\tag{C1}$$

where

$$\mathbf{x}_{\text{C}}^{(n)} = \left\{x_{\text{C},h}^{(n)}\right\}_{h=-1+\delta_{n,0}}^{+\infty}\tag{C2a}$$

$$\mathbf{x}_{\text{D}}^{(n)} = \left\{x_{\text{D},h}^{(n)}\right\}_{h=0}^{+\infty}\tag{C2b}$$

and

$$x_{\text{C},-1}^{(n)} = \frac{\gamma_{\text{C},-1}^{(n)}}{\hat{\alpha}^{(n)}},\quad \text{for } n\neq 0\tag{C3a}$$

$$x_{T,h}^{(n)} = \gamma_{T,h}^{(n)},\quad \text{for } h>0\tag{C3b}$$

$$\hat{\alpha}^{(n)} = \frac{1}{\sqrt{1-(\alpha^{(n)})^2/(\text{j}2\omega\varepsilon_0 R)}}.\tag{C3c}$$

The coefficient matrix is

$$\mathbf{A}^{(n)} = \begin{bmatrix}\text{j}\frac{1}{2\omega\varepsilon_0}\mathbf{A}_{\text{C,C}}^{(n)} & \text{j}\sqrt{\frac{-\text{j}R}{2\omega\varepsilon_0}}\mathbf{A}_{\text{C,D}}^{(n)}\\ -\text{j}\sqrt{\frac{-\text{j}R}{2\omega\varepsilon_0}}\mathbf{A}_{\text{D,C}}^{(n)} & -R\mathbf{A}_{\text{D,D}}^{(n)}\end{bmatrix}\tag{C4}$$

where

$$\mathbf{A}_{\text{C,C}}^{(n)} = \left\{A_{\text{C,C},k,h}^{(n)}\right\}_{k,h=-1+\delta_{n,0}}^{+\infty}\tag{C5a}$$

$$\mathbf{A}_{\text{C,D}}^{(n)} = \left\{A_{\text{C,D},k,h}^{(n)}\right\}_{k=-1+\delta_{n,0},h=0}^{+\infty}\tag{C5b}$$

$$\mathbf{A}_{\text{D,C}}^{(n)} = \left\{A_{\text{D,C},k,h}^{(n)}\right\}_{k=0,h=-1+\delta_{n,0}}^{+\infty}\tag{C5c}$$

$$\mathbf{A}_{\text{D,D}}^{(n)} = \left\{A_{\text{D,D},k,h}^{(n)}\right\}_{k,h=0}^{+\infty}\tag{C5d}$$

and

$$A_{\text{C,C},-1,-1}^{(n)} = \left(\hat{\alpha}^{(n)}\right)^2\left[M_{\text{C},-1,-1}^{(n)}-\left(\alpha^{(n)}\right)^2 M_{\text{D},-1,-1}^{(n)}\right]\quad \text{for } n\neq 0\tag{C6a}$$

$$A_{\text{C,C},-1,h}^{(n)} = A_{\text{C,C},h,-1}^{(n)} = \hat{\alpha}^{(n)}M_{\text{C},-1,h}^{(n)},\quad \text{for } n\neq 0,\ h\geq 0\tag{C6b}$$

$$A_{\text{C,C},k,h}^{(n)} = A_{\text{C,C},h,k}^{(n)} = M_{\text{C},k,h}^{(n)},\quad \text{for } k,h\geq 0\tag{C6c}$$

$$A_{\text{C,D},-1,h}^{(n)} = -A_{\text{D,C},h,-1}^{(n)} = -\hat{\alpha}^{(n)}\alpha^{(n)}M_{\text{D},-1,h}^{(n)}\quad \text{for } n\neq 0,\ h\geq 0\tag{C6d}$$

$$A_{\text{C,D},k,h}^{(n)} = A_{\text{D,C},h,k}^{(n)} = 0,\quad \text{for } k,h\geq 0\tag{C6e}$$

$$A_{\text{D,D},k,h}^{(n)} = A_{\text{D,D},h,k}^{(n)} = M_{\text{D},k,h}^{(n)},\quad \text{for } k,h\geq 0\tag{C6f}$$

$$M_{T,k,h}^{(n)} = \int_0^{+\infty}\tilde{f}_{T,k}^{(n)}(w)\,\tilde{f}_{T,h}^{(n)}(w)\cdot\left(\frac{1}{\tilde{G}_T(w)-R}-\kappa_T w^{2(p_T-1)}\right)w\,dw.\tag{C6g}$$

The free-term vector is

$$\mathbf{c}^{(n)} = \begin{bmatrix} \mathrm{j}\dfrac{1}{\sqrt{2\omega\varepsilon_0}}\mathbf{c}_{\mathrm{C}}^{(m)} \\ -\mathrm{j}\sqrt{-\mathrm{j}R}\mathbf{c}_{\mathrm{D}}^{(m)} \end{bmatrix} \tag{C7}$$

where

$$\mathbf{c}_{\mathrm{C}}^{(n)} = \left\{c_{\mathrm{C},k}^{(n)}\right\}_{k=-1+\delta_{n,0}}^{+\infty} \tag{C8a}$$

$$\mathbf{c}_{\mathrm{D}}^{(n)} = \left\{c_{\mathrm{D},k}^{(n)}\right\}_{k=0}^{+\infty} \tag{C8b}$$

and

$$c_{\mathrm{C},-1}^{(n)} = \hat{\alpha}^{(n)}\left(b_{\mathrm{C},-1}^{(n)} - \alpha^{(n)} b_{\mathrm{D},-1}^{(n)}\right), \quad \text{for } n \neq 0 \tag{C9a}$$

$$c_{T,k}^{(n)} = b_{T,k}^{(n)}, \quad \text{for } k > 0 \tag{C9b}$$

$$b_{T,k}^{(n)} = -\mathrm{j}^{n+1} e^{-\mathrm{j}n\phi_0} E_{0t} \frac{\tilde{f}_{T,k}^{(n)}\left(k_0 s_{\theta_0}\right)}{\tilde{G}_T\left(k_0 s_{\theta_0}\right) - R}. \tag{C9c}$$

ACKNOWLEDGMENT

The authors thank Prof. Fulvio Schettino for providing the CST-MWS results for comparison. Alexander I. Nosich is grateful to Université de Rennes for the hospitality as a part of the program of solidarity with Ukraine.

REFERENCES

[1] J. W. Strutt, "On the passage of waves through apertures in plane screens, and allied problems," *Philos. Mag. J. Sci.*, vol. 43, no. 263, pp. 259–272, 1897.

[2] C. J. Bouwkamp, "Diffraction theory," *Rep. Prog. Phys.*, vol. 17, no. 1, pp. 35–100, 1954.

[3] J. J. Bowman, T. B. A. Senior, and P. L. E. Uslenghi, *Electromagnetic and Acoustic Scattering by Simple Shapes*. New York, NY, USA: Wiley, 1969.

[4] C. Butler, Y. Rahmat-Samii, and R. Mittra, "Electromagnetic penetration through apertures in conducting surfaces," *IEEE Trans. Electromagn. Compat.*, vol. EMC-20, no. 1, pp. 82–93, Feb. 1978.

[5] E. V. Jull, *Aperture Antennas and Diffraction Theory*. London, U.K.: Peter Peregrinus, 1981.

[6] K. Hongo and Q. A. Naqvi, "Diffraction of electromagnetic wave by disk and circular hole in a perfectly conducting plane," *Prog. Electromagn. Res.*, vol. 68, pp. 113–150, 2007.

[7] O. P. Bruno and S. K. Lintner, "A high-order integral solver for scalar problems of diffraction by screens and apertures in three-dimensional space," *J. Comput. Phys.*, vol. 252, pp. 250–274, Nov. 2013.

[8] K. A. Michalski and J. R. Mosig, "On the plane wave-excited subwavelength circular aperture in a thin perfectly conducting flat screen," *IEEE Trans. Antennas Propag.*, vol. 62, no. 4, pp. 2121–2129, Apr. 2014.

[9] G. Lovat, P. Burghignoli, R. Araneo, and S. Celozzi, "Magnetic field penetration through a circular aperture in a perfectly conducting plate excited by a coaxial loop," *IET Microw., Antennas Propag.*, vol. 15, no. 10, pp. 1147–1158, Aug. 2021.

[10] C. Jerez-Hanckes and J. Pinto, "Spectral Galerkin method for solving Helmholtz boundary integral equations on smooth screens," *IMA J. Numer. Anal.*, vol. 42, no. 4, pp. 3571–3608, Oct. 2022.

[11] H. Neugebauer, "Diffraction of electromagnetic waves caused by apertures in absorbing plane screens," *IRE Trans. Antennas Propag.*, vol. 4, no. 2, pp. 115–119, Apr. 1956.

[12] A. A. Ashour, "Electromagnetic induction in finite thin sheets," *Quart. J. Mech. Appl. Math.*, vol. 18, no. 1, pp. 73–86, 1965.

[13] E. Popov et al., "Single-scattering theory of light diffraction by a circular subwavelength aperture in a finitely conducting screen," *J. Opt. Soc. Amer. A, Opt. Image Sci.*, vol. 24, no. 2, pp. 339–358, 2007.

[14] G. Lovat, P. Burghignoli, R. Araneo, and S. Celozzi, "Axially symmetric source field penetration through a circular aperture in a thin impedance plate," *IEEE Trans. Antennas Propag.*, vol. 70, no. 9, pp. 8348–8359, Sep. 2022.

[15] A. I. Nosich, "Method of analytical regularization in computational photonics," *Radio Sci.*, vol. 51, no. 8, pp. 1421–1430, Aug. 2016.

[16] M. Lucido, K. Kobayashi, F. Medina, A. Nosich, and E. Vinogradova, "Guest editorial: Method of analytical regularisation for new frontiers of applied electromagnetics," *IET Microw., Antennas Propag.*, vol. 15, no. 10, pp. 1127–1132, Aug. 2021.

[17] M. Lucido, "Scattering by a tilted strip buried in a lossy half-space at oblique incidence," *Prog. Electromagn. Res. M*, vol. 37, pp. 51–62, 2014.

[18] M. Lucido, F. Schettino, M. D. Migliore, D. Pinchera, F. Di Murro, and G. Panariello, "Electromagnetic scattering by a zero-thickness PEC annular ring: A new highly efficient MoM solution," *J. Electromagn. Waves Appl.*, vol. 31, no. 4, pp. 405–416, Mar. 2017.

[19] M. Lucido, C. Santomassimo, and G. Panariello, "The method of analytical preconditioning in the analysis of the propagation in dielectric waveguides with wedges," *J. Lightw. Technol.*, vol. 36, no. 14, pp. 2925–2932, Jul. 15, 2018.

[20] M. Lucido, M. V. Balaban, and A. I. Nosich, "Plane wave scattering from thin dielectric disk in free space: Generalized boundary conditions, regularizing Galerkin technique and whispering gallery mode resonances," *IET Microw., Antennas Propag.*, vol. 15, no. 10, pp. 1159–1170, Aug. 2021.

[21] M. Lucido, M. V. Balaban, and A. I. Nosich, "Terahertz-range plasmon and whispering gallery mode resonances in the plane wave scattering from thin microsize dielectric disk with graphene covers," *Proc. Roy. Soc. A, Math., Phys. Eng. Sci.*, vol. 478, no. 2262, Jun. 2022.

[22] M. Lucido, F. Di Murro, and G. Panariello, "Electromagnetic scattering from a zero-thickness PEC disk: A note on the Helmholtz-Galerkin analytically regularizing procedure," *Prog. Electromagn. Res. Lett.*, vol. 71, pp. 7–13, 2017.

[23] M. Lucido, F. Schettino, and G. Panariello, "Scattering from a thin resistive disk: A guaranteed fast convergence technique," *IEEE Trans. Antennas Propag.*, vol. 69, no. 1, pp. 387–396, Jan. 2021.

[24] E. H. Bleszynski, M. K. Bleszynski, and T. Jaroszewicz, "Surface-integral equations for electromagnetic scattering from impenetrable and penetrable sheets," *IEEE Antennas Propag. Mag.*, vol. 35, no. 6, pp. 14–24, Dec. 1993.

[25] D. S. Jones, *The Theory Electromagnetism*. New York, NY, USA: Pergamon, 1964.

[26] D. Colton and R. Kress, *Integral Equation Methods Scattering Theory*. New York, NY, USA: Wiley, 1983.

[27] W. C. Chew and J. A. Kong, "Resonance of nonaxial symmetric modes in circular microstrip disk antenna," *J. Math. Phys.*, vol. 21, no. 10, pp. 2590–2598, 1980.

[28] M. Abramowitz and I. A. Stegun, *Handbook Math. Functions*. Frankfurt, Germany: Verlag Harri Deutsch, 1984.

[29] M. V. Balaban, R. Sauleau, T. M. Benson, and A. I. Nosich, "Dual integral equations technique in electromagnetic wave scattering by a thin disk," *Prog. Electromagn. Res. B*, vol. 16, pp. 107–126, 2009.

[30] S. Gradstein and I. M. Ryzhik, *Tables of Integrals, Series and Products*. New York, USA: Academic, 2000.

[31] I. M. Braver, P. S. Fridberg, K. L. Garb, and I. M. Yakover, "The behavior of the electromagnetic field near the edge of a resistive half-plane," *IEEE Trans. Antennas Propag.*, vol. 36, no. 12, pp. 1760–1768, Dec. 1988.

[32] E. C. Titchmarsh, *Introduction to the Theory of Fourier Integrals*. London, U.K.: Oxford Univ. Press, 1948.

[33] J. Van Bladel, "A discussion of Helmholtz' theorem on a surface," *Archiv Elektronik Übertragungstechnik*, vol. 47, no. 3, pp. 131–136, 1993.

[34] M. Lucido, M. V. Balaban, S. Dukhopelnykov, and A. I. Nosich, "A fast-converging scheme for the electromagnetic scattering from a thin dielectric disk," *Electronics*, vol. 9, no. 9, p. 1451, Sep. 2020.

[35] J. E. Wilkins, "Neumann series of Bessel functions," *Trans. Amer. Math. Soc.*, vol. 64, no. 2, pp. 359–385, 1948.

[36] P. J. Davis and P. Rabinowitz, *Methods of Numerical Integration*, 2nd ed. New York, NY, USA: Academic, 1984.

[37] N. Geng and L. Carin, "Wide-band electromagnetic scattering from a dielectric BOR buried in a layered lossy dispersive medium," *IEEE Trans. Antennas Propag.*, vol. 47, no. 4, pp. 610–619, Apr. 1999.

[38] A. I. Nosich, "Radiation conditions, limiting absorption principle, and general relations in open waveguide scattering," *J. Electromagn. Waves Appl.*, vol. 8, no. 3, pp. 329–353, Jan. 1994.

[39] C. Müller, *Foundations of the Mathematical Theory of Electromagnetic Waves*. Berlin, Germany: Springer, 1969.

Mario Lucido (Senior Member, IEEE) was born in Naples, Italy, in 1972. He received the Laurea degree (summa cum laude) in electronic engineering from the University of Naples Federico II, Naples, in 2000, and the Ph.D. degree in electrical and telecommunication engineering from the University of Cassino and Southern Lazio (UNICAS), Cassino, Italy, in 2004.

Since 2005, he has been with UNICAS, where he is currently an Associate Professor of electromagnetic fields. He has authored about 100 scientific journal articles and conference papers. His research interests include semi-analytical techniques for the analysis of diffraction and scattering problems, waveguide and optical waveguide propagation, microwave circuits, microstrip antennas, and open resonators.

Dr. Lucido is a Senior Member of the International Union of Radio Science (URSI), and a member of several societies, consortia, and research centers. He serves as an International Advisory Board Member of the Editorial Board of *Radiophysics and Electronics* Journal, an Associate Editor of *IET Microwave, Antennas and Propagation* (IET-MAP) and *International Journal of Applied Electromagnetics and Mechanics*, an Editorial Board Member of *Applied Sciences* and *Academia Engineering*, and a referee for several scientific journals and international conferences. He was a Lead Guest Editor of the Special Issue of IET-MAP titled "Method of Analytical Regularization for New Frontiers of Applied Electromagnetics," a Guest Editor of the Special Issue of *Applied Sciences* titled "Advances in Analytical-Numerical Techniques for Planar Microwave Circuits and Microstrip Antennas," and he is currently the Lead Guest Editor of the Special Issue of *Applied Sciences* titled "Challenge of Guaranteed Convergence in Applied Electromagnetics: Recent Progress in the Methods of Analytical Regularization." He received the "Giorgio Barzilai" Prize for the Best Young Scientist Paper at the Italian National Congress on Electromagnetics (RiNEm) in 2006 and the "Volodymyr G. Sologub" senior researcher award for contribution to the development of analytical regularization methods in computational electromagnetics at the XVI IEEE International Conference on Mathematical Methods in Electromagnetic Theory (MMET) in 2016.

Alexander I. Nosich (Fellow, IEEE) was born in Kharkiv, Ukraine, in 1953. He received the M.S., Ph.D., and D.Sc. (higher research doctorate) degrees in radio physics from Kharkiv National University, Kharkiv, Ukraine, in 1975, 1979, and 1990, respectively.

Since 1979, he has been with the Institute of Radio-Physics and Electronics (IRE), National Academy of Sciences of Ukraine (NASU), Kharkiv, where he is currently the Professor and the Principal Scientist. He is also the Head of the Laboratory of Micro and Nano Optics, founded by him in 2010. Since 1992, he has held numerous guest fellowships and professorships in the EU, Japan, Singapore, Turkey, and the U.K. He has authored and coauthored over 200 journal articles and book chapters, the vast majority of which are related to the methods of analytical regularization. His research interests include the method of analytical regularization, Nystrom-type discretization methods, wave scattering, and eigenvalue problems, open waveguides, open resonators, antennas, lasers, and the history of microwaves.

Dr. Nosich has been an Initiator and Technical Committee Chairman of the Biennial International Conference Series on Mathematical Methods in Electromagnetic Theory (IEEE MMET), held in Ukraine, since 1990. In parallel, in 1995, he organized the IEEE Antennas and Propagation Society East Ukraine Chapter, the first one in the former USSR. Later, he was representing Ukraine in the European Microwave Association (2001–2003) and the European Association on Antennas and Propagation (2006–2020). He was awarded the honorary title of Doctor Honoris Causa of the University of Rennes 1, France (2015), the Galileo Galilei Medal of the International Commission for Optics (2017), and fellow of the Optica (OSA) (2020). He was also a co-recipient of the 2017 National Prize of Ukraine in Science and Technology for the works titled, "Photonics of Semiconductor and Dielectric Nanostructures" and the 2018 Solomon I. Pekar Award of NASU in the solid-state physics theory. Since 2019, he serves as an Elected Member of the Academic Board of the National Research Foundation of Ukraine.

Open Access funding provided by 'Università degli Studi di Cassino e del Lazio Meridionale' within the CRUI CARE Agreement